Robust low-rank multilinear tensor approximation for a joint estimation of the multilinear rank and the loading matrices

Xu Han, Laurent Albera, *Senior Member, IEEE,* Amar Kachenoura, Huazhong Shu, *Senior Member, IEEE,* and Lotfi Senhadji, *Senior Member, IEEE*

Abstract—In order to compute the best low-rank tensor approximation using the Multilinear Tensor Decomposition (MTD) model, it is essential to estimate the rank of the underlying multilinear tensor from the noisy observation tensor. In this paper, we propose a Robust MTD (R-MTD) method, which jointly estimates the multilinear rank and the loading matrices. Based on the low-rank property and an over-estimation of the core tensor, this joint estimation problem is solved by promoting (group) sparsity of the over-estimated core tensor. Group sparsity is promoted using mixed-norms. Then we establish a link between the mixed-norms and the nuclear norm, showing that mixed-norms are better candidates for a convex envelope of the rank. After several iterations of the Alternating Direction Method of Multipliers (ADMM), the Minimum Description Length (MDL) criterion computed from the eigenvalues of the unfolding matrices of the estimated core tensor is minimized in order to estimate the multilinear rank. The latter is then used to estimate more accurately the loading matrices. We further develop another R-MTD method, called R-OMTD, by imposing an orthonormality constraint on each loading matrix in order to decrease the computation complexity. A series of simulated noisy tensor and real-world data are used to show the effectiveness of the proposed methods compared with state-of-the-art methods.

Index Terms—Low-rank multilinear tensor approximation, rank estimation, group sparsity, mixed-norms, minimum description length, ADMM.

1 Introduction

Tensor decompositions play an important role in various domains for several decades [1] such as in computer vision [2], [3], [4], [5], [6], [7], machine learning [8], [9], [10], signal processing [11], [12] and numerical linear algebra [13], [14], [15], [16], [17]. The Multilinear Tensor Decomposition (MTD) model was originally introduced by Tucker [18] and it received much attention. The most famous MTD method is the Higher-Order Singular Value Decomposition (HOSVD) method [15], which is a direct generalization of the matrix SVD method to tensors. An iterative and more efficient MTD method was proposed in [13], called Higher-Order Orthogonal Iteration (HOOI). However, HOOI cannot provide an excellent low-rank approximation in the presence of noise when the multilinear rank is over-estimated, say when the overfactoring problem is encountered. Hence, the rank estimation in the presence of noise is investigated in this paper. As well-known, the multilinear rank of a tensor can be estimated by looking for the major breaking point of the singular value curve of its unfolding matrices. Unfortunately, the latter problem is hard in the presence of noise for low Signal-to-Noise Ratio (SNR) values.

In order to overcome this drawback, some methods applied the information theoretic criterion for model selection, such as Bayesian Information Criterion (BIC) [19], LAPlace's method (LAP) [20] and Minimum Description Length (MDL) [21], [22]. Cichocki et al. [23] proposed to use the Second ORder sTatistic of the Eigenvalues (SORTE). The QDA procedure (Quotient of Differences in Additional values) [24] was also used as a judge-independent operationalization of the scree-test combined with the Kaiser criterion [25]. In addition, the balance between the fit of the approximation solution and the choice of the breaking point was considered in the DIFference in FIT (DIFFIT) [26] and MuLtilinear Rank ESTimate (MLREST) [27] methods. A good behavior of the aforementioned methods on rank estimation is attainable provided that the SNR value is high. The recent published SCORE (Sparse CORE tensor) method [28] introduced a modified eigenvalue-based method. The breaking point of the modified eigenvalues of the core tensor computed by means of the HOSVD algorithm [15] is found using the MDL criterion [22]. The SCORE method is more robust with respect to noise than classical techniques, but it is still sensitive to low SNR values. This occurs because all these methods estimate the multilinear rank of the noisy tensor instead of that of the denoised tensor.

Alternatively, authors proposed low-rank approximation methods without explicitly computing the multilinear rank. These techniques were applied on hyperspectral image and video data, such as the Low Rank Tensor Approximation (LRTA) [29], PARAllel FACtor analysis (PARAFAC) [30], tensor-Singular Value Decomposition (t-SVD) [31] and

- *X. Han, L.Albera, A. Kachenoura and L. Senhadji are with the INSERM, U1099, Rennes, F-35000, France and the LTSI, Université de Rennes 1,Rennes, F-35000, France, and also with the Centre de Recherche en Information Biomédicale Sino-Français (CRIBs), Rennes, F-35000, France (e-mail: hanxu.list@gmail.com; laurent.albera@univ-rennes1.fr; amar.kachenoura@univ-rennes1.fr; lotfi.senhadji@univ-rennes1.fr).*
- *H. Shu is with the Laboratory of Image Science and Technology, School of Computer Science and Engineering, Southeast University, Nanjing 210096, China, and also with the Centre de Recherche en Information Biomédicale SinoFrançais (CRIBs), Nanjing 210096, China (e-mail: shu.list@seu.edu.cn).*

Manuscriptxxxxxxxxxxxx received xx xx, xxxx; revised xx xx, xxxx.

Trace/TV norm (Trace/TV) [32] methods. Recently, Xie et al. [33] proposed a Kronecker-Basis-Representation (KBR) method, which imposes a low-rank constraint on each unfolding matrix of the noisy tensor and which promotes sparsity of the over-estimated core tensor in order to denoise it. The performance of KBR is not only better than the other low-rank approximation methods, but it is also more efficient from an application point of view than i) the dictionary learning methods such as K-SVD [34], [35] and TDL (Tensor Dictionary Learning) [4], and ii) the block matching and filter techniques such as BM3D (Block-Matching and 3-D filtering) [36], BM4D [37] [38] and ANLM (Adaptive Non-Local Means filter) [39]. Albeit the intrinsic physical interpretation of the MTD model by means of the KBR method generated much attention, KBR has certain drawbacks. More particularly, KBR imposes the low-rank property by minimizing the nuclear norm, which is not the most rational choice as explained in section 3. Moreover, KBR preserves the over-estimated status of the core tensor over the iterations and it is not sufficiently robust with the presence of noise.

In this paper, we propose a 2-step Robust MTD (R-MTD) method. The first step is designed to estimate the multilinear rank based on the low-rank property and on over-estimation of the core tensor. More particularly, (group) sparsity of the over-estimated core tensor is promoted using mixed and l_1 norms, respectively. The second step uses the estimated multilinear rank to estimate accurately the loading matrices. To support our work, we establish a link between the mixed norm and the nuclear norm, showing that mixed norms are better candidates for a convex envelope of the rank. We provide the details of the R-MTD algorithm and a computational complexity analysis. Furthermore, another robust MTD method imposing an Orthonormal constraint on each loading matrix is also proposed, namely R-OMTD, which is more robust with respect to the presence of noise and much faster than R-MTD. A series of simulated noisy tensor and real-world data are used to show the effectiveness of the proposed methods in comparison with classical techniques.

The paper is organized as follows. Section II lists some necessary notations. The theoretical analysis showing the interest in using mixed norms instead of the nuclear norm is presented in Section III. In Section IV, we introduce the iterative R-MTD and R-OMTD methods, including a computational complexity analysis. Section V gives the computer results. The conclusion is drawn in the last section.

2 Notations

A scalar is denoted by an italic letter, e.g. x and I. A vector is denoted by a bold lowercase letter, e.g. $\mathbf{x} \in \mathbb{R}^I$, a matrix is represented by a bold capital letter, e.g. $\mathbf{X} \in \mathbb{R}^{I\times J}$, and $\mathbf{I}$ stands for the identity matrix. The symbols $\mathbf{X}_{i,:}$ and $\mathbf{X}_{:,j}$ denote the i-th row and j-th column of $\mathbf{X}$, respectively. The vectorization of $\mathbf{X}$ is denoted by $\text{vec}(\mathbf{X}) \in \mathbb{R}^{IJ\times 1}$. $\mathbf{X}^\dagger$ is the pseudo-inverse of matrix $\mathbf{X}$. The nuclear norm of a matrix $\mathbf{X} \in \mathbb{R}^{I\times J}$ with rank r is equal to the sum of its singular values, i.e. $\|\mathbf{X}\|_* = \sum_{i=1}^r \sigma_i$, and $\|\mathbf{X}\|$ is the largest singular value of $\mathbf{X}$. The l_0, l_1 and Frobenius norms of $\mathbf{X} \in \mathbb{R}^{I\times J}$ are defined by $\|\mathbf{X}\|_0 = \sum_{i=1}^I \sum_{j=1}^J \mathbf{X}_{i,j}/\mathbf{X}_{i,j}$ with $\mathbf{X}_{i,j} \neq 0$, $\|\mathbf{X}\|_1 = \sum_{i=1}^I \sum_{j=1}^J |\mathbf{X}_{i,j}|$ and $\|\mathbf{X}\|_F = \sqrt{\sum_{i=1}^I \sum_{j=1}^J \mathbf{X}_{i,j}^2}$, respectively. The mixed-norms of $\mathbf{X} \in \mathbb{R}^{I\times J}$ are given by:

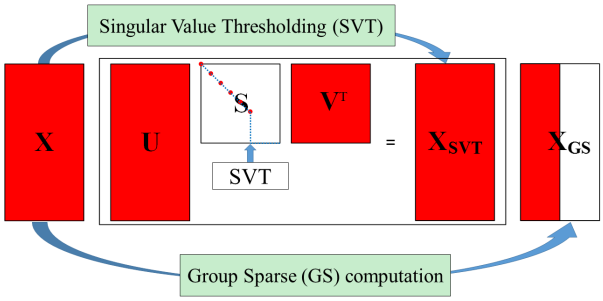

Fig. 1: Two ways of promoting the low-rank property (zero components are in white)

$$\|\mathbf{X}\|_{2,1} = \sum_{i=1}^I \sqrt{\sum_{j=1}^J \mathbf{X}_{i,j}^2} = Tr[\mathbf{X}^\intercal \mathbf{\Phi} \mathbf{X}]$$

and:

$$\|\mathbf{X}\|_{1,2} = \sum_{j=1}^J \sqrt{\sum_{i=1}^I \mathbf{X}_{i,j}^2} = Tr[\mathbf{X} \mathbf{\Psi} \mathbf{X}^\intercal]$$

where $Tr[.]$ is the trace operator, where $\mathbf{\Phi}$ is a diagonal matrix with $\mathbf{\Phi}_{i,i} = 1/\sqrt{\sum_{j=1}^J \mathbf{X}_{i,j}^2}$ and where $\mathbf{\Psi}$ is a diagonal matrix with $\mathbf{\Psi}_{j,j} = 1/\sqrt{\sum_{i=1}^I \mathbf{X}_{i,j}^2}$. Note that these compact formulas are convenient for an iterative convex optimization for which $\mathbf{\Phi}$ ($\mathbf{\Psi}$ respectively) and $\mathbf{X}$ are updated alternatively.

A higher-order tensor is symbolized by a bold calligraphic letter, e.g., $\boldsymbol{\mathcal{X}} \in \mathbb{R}^{I_1\times I_2\times\cdots\times I_N}$. The sub-tensor $\boldsymbol{\mathcal{X}}_{i_n=k}$ is obtained by fixing the n-th index to k. The scalar product of two tensors $\boldsymbol{\mathcal{X}}$ and $\boldsymbol{\mathcal{Y}}$ of size $I_1 \times I_2 \times \cdots \times I_N$ is defined by:

$$\langle \boldsymbol{\mathcal{X}}, \boldsymbol{\mathcal{Y}} \rangle = \sum_{i_1=1}^{I_1} \cdots \sum_{i_N=1}^{I_N} \boldsymbol{\mathcal{X}}_{i_1,\cdots,i_N} \boldsymbol{\mathcal{Y}}_{i_1,\cdots,i_N}$$

The Frobenius norm of tensor $\boldsymbol{\mathcal{X}}$ is defined by $\|\boldsymbol{\mathcal{X}}\|_F = \sqrt{\sum_{i_1\ldots i_N} \boldsymbol{\mathcal{X}}_{i_1,\ldots,i_N}^2}$. The sign "$\otimes$" denotes the Kronecker product operator. The n-th mode unfolding matrix of tensor $\boldsymbol{\mathcal{X}} \in \mathbb{R}^{I_1\times I_2\times\cdots\times I_N}$ is denoted by $\mathbf{X}^{(n)} \in \mathbb{R}^{I_n\times(I_{n+1}I_{n+2}\ldots I_N I_1 I_2 \ldots I_{n-1})}$. The n-th mode product of a tensor $\boldsymbol{\mathcal{X}}$ by a matrix $\mathbf{U} \in \mathbb{R}^{J_n\times I_n}$, denoted by $\boldsymbol{\mathcal{X}} \times_n \mathbf{U}$, is a tensor of size $I_1 \times \cdots \times I_{n-1} \times J_n \times I_{n+1} \times \cdots \times I_N$ and it is computed by:

$$(\boldsymbol{\mathcal{X}} \times_n \mathbf{U})_{i_1,\ldots,j_n,\ldots,i_N} = \sum_{i_n=1}^{I_N} \boldsymbol{\mathcal{X}}_{i_1,\ldots,i_n,\ldots,i_N} \mathbf{U}_{j_n,i_n}$$

Equivalently, the above product can be calculated by tensorizing the following matrix multiplication $(\boldsymbol{\mathcal{X}} \times_n \mathbf{U})^{(n)} = \mathbf{U}\mathbf{X}^{(n)}$. The MTD model of multilinear rank (R_1, R_2, R_3) of the third order tensor $\mathcal{T}$ is denoted by:

$$\mathcal{T} = \mathcal{G} \times_1 \mathbf{A} \times_2 \mathbf{B} \times_3 \mathbf{C} + \mathcal{N} = [\![\mathcal{G}; \mathbf{A}, \mathbf{B}, \mathbf{C}]\!] + \mathcal{N}$$

where $\mathcal{G}$ is the core tensor, where $\mathbf{A}$, $\mathbf{B}$, $\mathbf{C}$ are the loading matrices and where $\mathcal{N}$ is the noise.

3 Theorem Framework

In this section, we first make an inventory of the different ways of computing a low-rank solution. Afterwards, we show why the mixed-norms should be preferred to promote

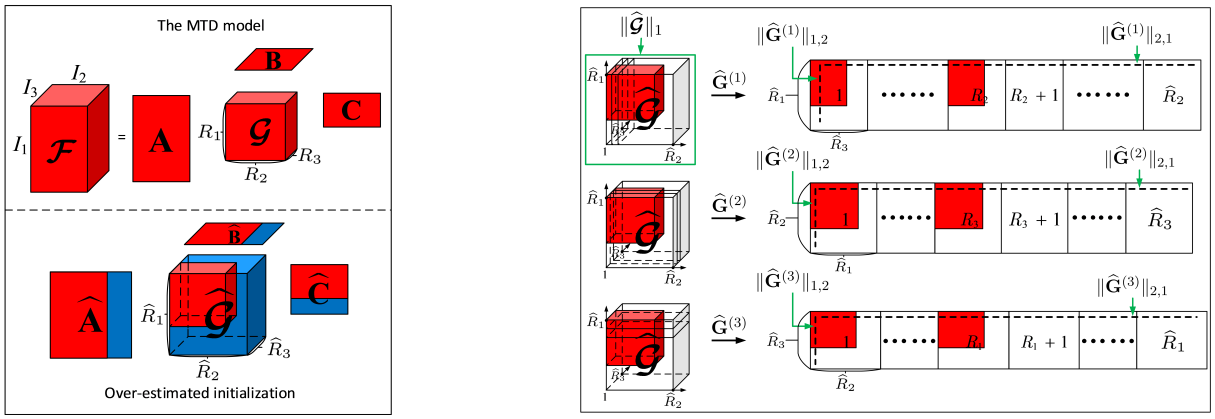

(a) (b)

Fig. 2: (a) The MTD model of a three-way array and its over-estimated version with $R_i \ll \widehat{R}_i \leq I_i$, for $i \in \{1, 2, 3\}$; (b) l_1 and mixed-norms applied to the core tensor in order to promote global and group sparsity, respectively.

group sparsity and to solve the low-rank estimation problem. Finally, we explain the interest in using the additional l_1 norm in order to promote global sparsity.

3.1 Bibliographical survey

The direct minimization of the rank is considered to be a NP-hard problem [40] and the works in [40], [41] show that the nuclear norm over the unit ball, i.e. $\|\mathbf{X}\| \leq 1$, is a convex envelop of the rank. Therefore, promoting the low-rank constraint can be achieved by using the nuclear norm [2], [3], [8], [7], [42], [43] by means of Singular Value Thresholding (SVT) [44], [45], [46], [47], [48] as displayed in Fig 1. Undoubtedly, these methods guarantee the low-rank property of the final solution but they do not ensure its group sparsity. Hence the use of the mixed-norms in order to promote simultaneously the low-rank and group sparsity properties.

3.2 Trump card of mixed-norms

Firstly, let's recall the definition of a convex envelope:

Definition 1. (Convex envelope). *Let f: $\mathbb{R}^n \rightarrow \mathbb{R}$ be a real-valued function. The convex envelope of f is the convex pointwise largest function $\mathcal{C}_f$: $\mathbb{R}^n \rightarrow \mathbb{R}$ which is pointwise less than f. In other words,* we have $\mathcal{C}_f = sup\{g$: $\mathbb{R}^n \rightarrow \mathbb{R} \,|\, g$ is convex and $\forall x \in \mathbb{R}^n, g(x) \leq f(x)\}$.

The first hinge between the nuclear norm and the mixed-norm $\|.\|_{2,1}$ was established in [49, proposition 1] for a thin matrix, i.e. for a matrix $\mathbf{X} \in \mathbb{R}^{m \times n}$ such as $m>n$. In this section, we first generalize this result through theorem 1 and corollary 1.

Theorem 1. *Given any matrix $\mathbf{X} \in \mathbb{R}^{m \times n}$ and its orthonormal subspace decompositions denoted by $\mathbf{X} = \mathbf{D}\boldsymbol{\alpha}$ and $\mathbf{X} = \boldsymbol{\theta}\mathbf{Z}$, where $\mathbf{D} \in \mathbb{R}^{m \times m}$ and $\mathbf{Z} \in \mathbb{R}^{n \times n}$ are orthonormal matrices, with $\boldsymbol{\alpha} \in \mathbb{R}^{m \times n}$ and $\boldsymbol{\theta} \in \mathbb{R}^{m \times n}$, the mixed-norms of $\boldsymbol{\alpha}$ and $\boldsymbol{\theta}$ are larger than or equal to the nuclear norm of $\mathbf{X}$, i.e. $\|\boldsymbol{\alpha}\|_{2,1} \geq \|\mathbf{X}\|_*$ and $\|\boldsymbol{\theta}\|_{1,2} \geq \|\mathbf{X}\|_*$.*

The proof is given in Appendix A. Then we can easily derive the following corollary by fixing $\mathbf{D}$ and $\mathbf{Z}$ to the identity matrix in theorem 1.

Corollary 1. *We have $\|\mathbf{X}\|_{2,1} \geq \|\mathbf{X}\|_*$ and $\|\mathbf{X}\|_{1,2} \geq \|\mathbf{X}\|_*$.*

It is deserved to note that both mixed-norms over the unit ball are better candidates than the nuclear norm for the convex envelope of rank when the matrix is with full row/column rank according to definition 1 and theorem 2.

Theorem 2. *Given any matrix $\mathbf{X} \in \mathbb{R}^{m \times n}$ with linearly independent rows or columns, we have:*

1) $\text{rank}(\mathbf{X}) \geq \frac{\|\mathbf{X}\|_{2,1}}{\|\mathbf{X}\|} \geq \frac{\|\mathbf{X}\|_*}{\|\mathbf{X}\|}$ *if $\mathbf{X}$ is full row rank.*

2) $\text{rank}(\mathbf{X}) \geq \frac{\|\mathbf{X}\|_{1,2}}{\|\mathbf{X}\|} \geq \frac{\|\mathbf{X}\|_*}{\|\mathbf{X}\|}$ *if $\mathbf{X}$ is full column rank.*

The proof is given in Appendix B. Furthermore, as well-known, the mixed-norms promote group sparsity, which is a very good trump card as used in section 4.

3.3 Additional use of the l_1 norm

The l_1 norm is a convex relaxation form of the l_0 norm [50], [33], [51], [52]. The minimization of the l_1 norm in addition to the mixed-norms will ensure a global sparsity and it will improve the robustness with respect to noise.

3.4 Model construction

The proposed model aims at estimating the multilinear rank of a tensor from its noisy observation by over-estimating the size $R_1 \times R_2 \times R_3$ of the core tensor $\boldsymbol{\mathcal{G}}$ as displayed in Fig. 2 (a). For the sake of simplicity, our methods are presented for third order tensors, but they can be easily extended to deal with higher order tensors. More particularly, the over-estimated core tensor $\widehat{\boldsymbol{\mathcal{G}}} \in \mathbb{R}^{\widehat{R}_1 \times \widehat{R}_2 \times \widehat{R}_3}$ should be group sparse. Then it can be computed by minimizing the mixed-norms of its unfolding matrices $\widehat{\mathbf{G}}^{(i)}$ as displayed in Fig. 2 (b). Moreover, the unfolding matrix $\widehat{\mathbf{G}}^{(i)}$ is full row rank so that the mixed-norm $\left\|\widehat{\mathbf{G}}^{(i)}\right\|_{2,1}$ in Fig. 2 (b) is more appropriate to be the convex envelop of the rank than the nuclear norm based on theorem 2. It is noteworthy that although the mixed-norm $\left\|\widehat{\mathbf{G}}^{(i)}\right\|_{1,2}$ is not appropriate to be the convex envelope of the rank, it should be adopted as an upper bound of the nuclear norm. Indeed we can show that it has the same minimum value as the nuclear norm when each component of the objective matrix is zero, thus the minimization of $\left\|\widehat{\mathbf{G}}^{(i)}\right\|_{1,2}$ will also minimize the nuclear

norm and consequently the rank. In addition, we minimize $\|\widehat{\mathcal{G}}\|_1$ as shown in Fig. 2 (b) in order to promote the global sparsity of the core tensor.

4 Proposed Methods

In order to guarantee a sufficient group sparsity of each unfolding matrix of $\widehat{\mathcal{G}}$, every rank R_i should be smaller than I_i as much as possible. In addition, since each unfolding matrix of $\mathcal{G}$ is full row rank, R_i should be smaller compared with $\prod_{k=1,k\neq i}^{3} R_k$, $i = 1, 2, 3$. Hence the following assumption made in the sequel:

$$R_i \leq \prod_{k=1,k\neq i}^{3} R_k \quad \text{and} \quad R_i \ll \min\{I_i, \prod_{k=1,k\neq i}^{3} I_k\}, i = 1, 2, 3.$$

4.1 The R-MTD method

The two steps of R-MTD are introduced in this section, including a computational complexity analysis.

4.1.1 R-MTD for rank estimation

The first considered minimization problem promotes (group) sparsity of the over-estimated core tensor as depicted in Fig. 2 (a), and it is given by:

$$\begin{aligned}\min_{\widehat{\mathbf{A}},\widehat{\mathbf{B}},\widehat{\mathbf{C}},\widehat{\mathcal{G}}} \ & \sum_{i=1}^{3} \lambda_i \Big(\big\|\widehat{\mathbf{G}}^{(i)}\big\|_{2,1} + \big\|\widehat{\mathbf{G}}^{(i)}\big\|_{1,2} \Big) + \big\|\widehat{\mathcal{G}}\big\|_1 \\ \text{s.t.} \ & \mathcal{T} = \widehat{\mathcal{G}} \times_1 \widehat{\mathbf{A}} \times_2 \widehat{\mathbf{B}} \times_3 \widehat{\mathbf{C}}, \widehat{\mathcal{G}} \in \mathbb{R}^{\widehat{R}_1 \times \widehat{R}_2 \times \widehat{R}_3}, \\ & \widehat{\mathbf{A}} \in \mathbb{R}^{I_1 \times \widehat{R}_1}, \widehat{\mathbf{B}} \in \mathbb{R}^{I_2 \times \widehat{R}_2}, \widehat{\mathbf{C}} \in \mathbb{R}^{I_3 \times \widehat{R}_3} \end{aligned} \tag{1}$$

The optimization algorithm to solve the above problem is the alternating direction method of multipliers (ADMM) [53], [54], [33], due to its easy implementations and good convergence properties. Problem (1) is then rewritten as follows:

$$\begin{aligned}\min_{\widehat{\mathbf{A}},\widehat{\mathbf{B}},\widehat{\mathbf{C}},\widehat{\mathcal{G}}} \ & \sum_{i=1}^{3} \lambda_i \Big(\big\|\widehat{\mathbf{G}}^{(i)}\big\|_{2,1} + \big\|\widehat{\mathbf{G}}^{(i)}\big\|_{1,2} \Big) + \big\|\widehat{\mathcal{P}}\big\|_1 \\ & + \frac{u}{2} \big\|\mathcal{T} - \widehat{\mathcal{G}} \times_1 \widehat{\mathbf{A}} \times_2 \widehat{\mathbf{B}} \times_3 \widehat{\mathbf{C}}\big\|_F^2 \\ \text{s.t.} \ & \widehat{\mathcal{G}} - \widehat{\mathcal{P}} = \mathbf{0} \end{aligned} \tag{2}$$

The augmented Lagrangian function $\mathcal{L}$ of (2) depending on the variables $(\widehat{\mathcal{G}}, \widehat{\mathbf{A}}, \widehat{\mathbf{B}}, \widehat{\mathbf{C}}, \widehat{\mathcal{P}}, \widehat{\mathcal{Y}}, \beta, \mathbf{\Phi}^{(i)}, \mathbf{\Psi}^{(i)})$ can be given with the following mixed-norm compact form:

$$\begin{aligned}\mathcal{L} = & \sum_{i=1}^{3} \lambda_i \Big[Tr\big(\widehat{\mathbf{G}}^{(i)^\intercal} \mathbf{\Phi}^{(i)} \widehat{\mathbf{G}}^{(i)}\big) + Tr\big(\widehat{\mathbf{G}}^{(i)} \mathbf{\Psi}^{(i)} \widehat{\mathbf{G}}^{(i)^\intercal}\big) \Big] \\ & + \big\|\widehat{\mathcal{P}}\big\|_1 + \frac{u}{2} \big\|\mathcal{T} - \widehat{\mathcal{G}} \times_1 \widehat{\mathbf{A}} \times_2 \widehat{\mathbf{B}} \times_3 \widehat{\mathbf{C}}\big\|_F^2 \\ & + \Big\langle \widehat{\mathcal{G}} - \widehat{\mathcal{P}}, \widehat{\mathcal{Y}} \Big\rangle + \frac{\beta}{2} \big\|\widehat{\mathcal{G}} - \widehat{\mathcal{P}}\big\|_F^2 \end{aligned} \tag{3}$$

where λ_i, u, β are the weighting coefficients and where $\widehat{\mathcal{Y}}$ is the tensor Lagrangian multiplier. The diagonal matrices $\mathbf{\Phi}^{(i)}$ and $\mathbf{\Psi}^{(i)}$ are given by $\mathbf{\Phi}^{(i)}_{m,m} = 1/\sqrt{\sum_{n=1}^{\prod_{k=1,k\neq i}^{3} \widehat{R}_k} (\widehat{\mathbf{G}}^{(i)}_{m,n})^2}$ and $\mathbf{\Psi}^{(i)}_{n,n} = 1/\sqrt{\sum_{m=1}^{\widehat{R}_i} (\widehat{\mathbf{G}}^{(i)}_{m,n})^2}$, respectively.

Now, let's derive the update rule of each variable. Regarding the first mode unfolding matrix of $\widehat{\mathcal{G}}$, its update rule is obtained by vanishing the following gradient equation of $\mathcal{L}$ with respect to $\widehat{\mathbf{G}}^{(1)}$:

$$\begin{aligned}\frac{\partial \mathcal{L}}{\partial \widehat{\mathbf{G}}^{(1)}} = & 2\lambda_1 \mathbf{\Phi}^{(1)} \widehat{\mathbf{G}}^{(1)} + 2\lambda_1 \widehat{\mathbf{G}}^{(1)} \mathbf{\Psi}^{(1)} + \beta \widehat{\mathbf{G}}^{(1)} \\ & + u \widehat{\mathbf{A}}^\intercal \widehat{\mathbf{A}} \widehat{\mathbf{G}}^{(1)} \big(\widehat{\mathbf{B}} \otimes \widehat{\mathbf{C}}\big)^\intercal \big(\widehat{\mathbf{B}} \otimes \widehat{\mathbf{C}}\big) + \widehat{\mathbf{Y}}^{(1)} \\ & - \beta \widehat{\mathbf{P}}^{(1)} - u \widehat{\mathbf{A}}^\intercal \mathbf{T}^{(1)} \big(\widehat{\mathbf{B}} \otimes \widehat{\mathbf{C}}\big) \end{aligned} \tag{4}$$

Based on the solution of the Encapsulating Sum given in [55], the $(k+1)$-th iteration of $\widehat{\mathbf{G}}^{(1)}$ can be computed as follows:

$$\begin{aligned}\mathrm{vec}(\widehat{\mathbf{G}}^{(1)}_{k+1}) = & \Big\{ \mathbf{I} \otimes \big(2\lambda_1 \mathbf{\Phi}^{(1)}_k\big) + \big(2\lambda_1 \mathbf{\Psi}^{(1)}_k + \beta_k \mathbf{I}\big) \otimes \mathbf{I} + \\ & \Big[\big(\widehat{\mathbf{B}}_k \otimes \widehat{\mathbf{C}}_k\big)^\intercal \big(\widehat{\mathbf{B}}_k \otimes \widehat{\mathbf{C}}_k\big) \Big] \otimes \big(u \widehat{\mathbf{A}}_k^\intercal \widehat{\mathbf{A}}_k\big) \Big\}^{-1} \mathrm{vec} \Big[\beta_k \widehat{\mathbf{P}}^{(1)}_k \\ & - \widehat{\mathbf{Y}}^{(1)}_k + u \widehat{\mathbf{A}}_k^\intercal \mathbf{T}^{(1)} \big(\widehat{\mathbf{B}}_k \otimes \widehat{\mathbf{C}}_k\big) \Big] \end{aligned} \tag{5}$$

Similarly, $\widehat{\mathbf{G}}^{(2)}$ and $\widehat{\mathbf{G}}^{(3)}$ can be updated as follows:

$$\begin{aligned}\mathrm{vec}(\widehat{\mathbf{G}}^{(2)}_{k+1}) = & \Big\{ \mathbf{I} \otimes \big(2\lambda_2 \mathbf{\Phi}^{(2)}_k\big) + \big(2\lambda_2 \mathbf{\Psi}^{(2)}_k + \beta_k \mathbf{I}\big) \otimes \mathbf{I} + \\ & \Big[\big(\widehat{\mathbf{C}}_k \otimes \widehat{\mathbf{A}}_k\big)^\intercal \big(\widehat{\mathbf{C}}_k \otimes \widehat{\mathbf{A}}_k\big) \Big] \otimes \big(u \widehat{\mathbf{B}}_k^\intercal \widehat{\mathbf{B}}_k\big) \Big\}^{-1} \mathrm{vec} \Big[\beta_k \widehat{\mathbf{P}}^{(2)}_k \\ & - \widehat{\mathbf{Y}}^{(2)}_k + u \widehat{\mathbf{B}}_k^\intercal \mathbf{T}^{(2)} \big(\widehat{\mathbf{C}}_k \otimes \widehat{\mathbf{A}}_k\big) \Big] \end{aligned} \tag{6}$$

$$\begin{aligned}\mathrm{vec}(\widehat{\mathbf{G}}^{(3)}_{k+1}) = & \Big\{ \mathbf{I} \otimes \big(2\lambda_3 \mathbf{\Phi}^{(3)}_k\big) + \big(2\lambda_3 \mathbf{\Psi}^{(3)}_k + \beta_k \mathbf{I}\big) \otimes \mathbf{I} + \\ & \Big[\big(\widehat{\mathbf{A}}_k \otimes \widehat{\mathbf{B}}_k\big)^\intercal \big(\widehat{\mathbf{A}}_k \otimes \widehat{\mathbf{B}}_k\big) \Big] \otimes \big(u \widehat{\mathbf{C}}_k^\intercal \widehat{\mathbf{C}}_k\big) \Big\}^{-1} \mathrm{vec} \Big[\beta_k \widehat{\mathbf{P}}^{(3)}_k \\ & - \widehat{\mathbf{Y}}^{(3)}_k + u \widehat{\mathbf{C}}_k^\intercal \mathbf{T}^{(3)} \big(\widehat{\mathbf{A}}_k \otimes \widehat{\mathbf{B}}_k\big) \Big] \end{aligned} \tag{7}$$

Note that $\mathbf{\Phi}^{(1)}_k$ and $\mathbf{\Psi}^{(1)}_k$ are computed from $\widehat{\mathbf{G}}^{(1)}_k$. The matirces $\mathbf{\Phi}^{(2)}_k$ and $\mathbf{\Psi}^{(2)}_k$ are calculated from $\widehat{\mathbf{G}}^{(1)}_{k+1}$. $\mathbf{\Phi}^{(3)}_k$ and $\mathbf{\Psi}^{(3)}_k$ are computed from $\widehat{\mathbf{G}}^{(2)}_{k+1}$.

Next, the update rule of the loading matrix $\widehat{\mathbf{A}}$ is obtained by vanishing the gradient of $\mathcal{L}$ with respect to $\widehat{\mathbf{A}}$:

$$\widehat{\mathbf{A}}_{k+1} = \mathbf{T}^{(1)} \Big[\widehat{\mathbf{G}}^{(1)}_{k+1} \big(\widehat{\mathbf{B}}_k \otimes \widehat{\mathbf{C}}_k\big)^\intercal \Big]^\dagger \tag{8}$$

In the same way, we have:

$$\widehat{\mathbf{B}}_{k+1} = \mathbf{T}^{(2)} \Big[\widehat{\mathbf{G}}^{(2)}_{k+1} \big(\widehat{\mathbf{C}}_k \otimes \widehat{\mathbf{A}}_{k+1}\big)^\intercal \Big]^\dagger \tag{9}$$

and

$$\widehat{\mathbf{C}}_{k+1} = \mathbf{T}^{(3)} \Big[\widehat{\mathbf{G}}^{(3)}_{k+1} \big(\widehat{\mathbf{A}}_{k+1} \otimes \widehat{\mathbf{B}}_{k+1}\big)^\intercal \Big]^\dagger \tag{10}$$

The update rule of $\widehat{\mathcal{P}}$ is derived by minimizing $\mathcal{L}$ with respect to $\widehat{\mathcal{P}}$:

$$\min_{\widehat{\mathcal{P}}} \big\|\widehat{\mathcal{P}}\big\|_1 + \Big\langle \widehat{\mathcal{G}} - \widehat{\mathcal{P}}, \widehat{\mathcal{Y}} \Big\rangle + \frac{\beta}{2} \big\|\widehat{\mathcal{G}} - \widehat{\mathcal{P}}\big\|_F^2 \tag{11}$$

which is equivalent to solve the following minimization problem:

$$\min_{\widehat{\mathcal{P}}} \big\|\widehat{\mathcal{P}}\big\|_1 + \frac{\beta}{2} \big\|\widehat{\mathcal{G}} - \widehat{\mathcal{P}} + \frac{1}{\beta} \widehat{\mathcal{Y}}\big\|_F^2 \tag{12}$$

A closed-solution of problems similar to (12) has been derived in [51], [52], leading to:

$$\widehat{\mathcal{P}}_{k+1} = \mathbb{S}_{\frac{1}{\beta_k}} \Big(\widehat{\mathcal{G}}_{k+1} + \frac{1}{\beta_k} \widehat{\mathcal{Y}}_k \Big) \tag{13}$$

where $\mathbb{S}_\tau(x) = \mathrm{sign}(x)(|x| - \tau, 0)$ for every real-valued variable x is the soft-thresholding operator and it is applied elementwise to the tensor $\widehat{\mathcal{G}}_{k+1} + \frac{1}{\beta_k} \widehat{\mathcal{Y}}_k$.

As far as the tensor multiplier $\widehat{\mathcal{Y}}$ is concerned, it is updated using the following ascent gradient rule:

$$\widehat{\mathcal{Y}}_{k+1} = \widehat{\mathcal{Y}}_k + \beta_k \big(\widehat{\mathcal{G}}_{k+1} - \widehat{\mathcal{P}}_{k+1}\big) \tag{14}$$

with

$$\beta_{k+1} = \rho \beta_k \tag{15}$$

where ρ is fixed strictly greater than 1. The proposed R-MTD algorithm is stopped when the following convergence criterion is satisfied:

$$\frac{\mathrm{error}_{k+1} - \mathrm{error}_k}{\mathrm{error}_k} < tolerance \tag{16}$$

where $\mathrm{error}_{k+1} = \big\|\mathcal{T} - [\![\widehat{\mathcal{G}}_{k+1}; \widehat{\mathbf{A}}_{k+1}, \widehat{\mathbf{B}}_{k+1}, \widehat{\mathbf{C}}_{k+1}]\!]\big\|_F$,

$\text{error}_k = \left\|\boldsymbol{\mathcal{T}} - [\![\widehat{\boldsymbol{\mathcal{G}}}_k; \widehat{\mathbf{A}}_k, \widehat{\mathbf{B}}_k, \widehat{\mathbf{C}}_k]\!]\right\|_F$ and where $tolerance$ is the threshold set by the user.

Finally, the rank R_i^{est} can be estimated by minimizing the MDL criterion [22], [21] built from the singular values $\lambda_p^{(i)}$ of the unfolding matrix $\widehat{\mathbf{G}}_{k+1}^{(i)}$ sorted in the descending order, i.e. $\lambda_1^{(i)} \geq \lambda_2^{(i)} \geq \cdots \geq \lambda_{\widehat{R}_i}^{(i)}$:

$$R_i^{est} = \arg\min_r -2\log\left\{\frac{\prod_{p=r+1}^{\widehat{R}_i}(\lambda_p^{(i)})^{1/(\widehat{R}_i-r)}}{\frac{1}{\widehat{R}_i-r}\sum_{p=r+1}^{\widehat{R}_i}\lambda_p^{(i)}}\right\}^{\prod_{k=1,k\neq i}^{3}\widehat{R}_k(\widehat{R}_i-r)} + r(2\widehat{R}_i - r)\log\Big(\prod_{k=1,k\neq i}^{3}\widehat{R}_k\Big), i = 1,2,3 \quad (17)$$

Let's explain how to initialize the loading matrices. The loading matrices $\widehat{\mathbf{A}} \in \mathbb{R}^{I_1\times I_1}, \widehat{\mathbf{B}} \in \mathbb{R}^{I_2\times I_2}$ and $\widehat{\mathbf{C}} \in \mathbb{R}^{I_3\times I_3}$ are orthonormal matrices obtained from the SVD of $\mathbf{T}^{(1)}$, $\mathbf{T}^{(2)}$ and $\mathbf{T}^{(3)}$. Thus, $\widehat{\mathbf{A}} = \mathbf{U}^{(1)}$, $\widehat{\mathbf{B}} = \mathbf{U}^{(2)}$ and $\widehat{\mathbf{C}} = \mathbf{U}^{(3)}$, where $\left[\mathbf{U}^{(i)}, \mathbf{S}^{(i)}, \mathbf{V}^{(i)}\right] = \text{svd}(\mathbf{T}^{(i)})$, $i = 1,2,3$. Based on [15, theorem 2], the core tensor can be computed as $\widehat{\boldsymbol{\mathcal{G}}} = \boldsymbol{\mathcal{T}} \times_1 \widehat{\mathbf{A}}^\intercal \times_2 \widehat{\mathbf{B}}^\intercal \times_3 \widehat{\mathbf{C}}^\intercal$ and the Frobenius norms of the sub-tensors of $\widehat{\boldsymbol{\mathcal{G}}}$ are in decreasing order, i.e. $\left\|\widehat{\boldsymbol{\mathcal{G}}}_{i_n=1}\right\|_F \geq \left\|\widehat{\boldsymbol{\mathcal{G}}}_{i_n=2}\right\|_F \geq \cdots \geq \left\|\widehat{\boldsymbol{\mathcal{G}}}_{i_n=I_n}\right\|_F, n = 1,2,3$. Consequently, the majority of components of $\widehat{\boldsymbol{\mathcal{G}}}$ with the large absolute values are concentrated in the red region as depicted in Fig. 2 (a) as wanted. Thus, the loading matrices can be initialized with $\mathbf{U}^{(1)}$, $\mathbf{U}^{(2)}$ and $\mathbf{U}^{(3)}$. Moreover, we can only select the first $\widehat{R}_1$, $\widehat{R}_2$ and $\widehat{R}_3$ columns of $\mathbf{U}^{(1)}$, $\mathbf{U}^{(2)}$ and $\mathbf{U}^{(3)}$, respectively, for a reduction of the computational complexity, i.e. $\widehat{\mathbf{A}}_0 = \mathbf{U}^{(1)}_{:,1:\widehat{R}_1}$, $\widehat{\mathbf{B}}_0 = \mathbf{U}^{(2)}_{:,1:\widehat{R}_2}$ and $\widehat{\mathbf{C}}_0 = \mathbf{U}^{(3)}_{:,1:\widehat{R}_3}$.

4.1.2 R-MTD for an estimation of the loading matrices

The estimated multilinear rank $(R_1^{est}, R_2^{est}, R_3^{est})$ is used and inserted in (1), leading to the following minimization problem:

$$\min_{\mathbf{A},\mathbf{B},\mathbf{C},\boldsymbol{\mathcal{G}}} \sum_{i=1}^{3}\lambda_i\Big(\left\|\mathbf{G}^{(i)}\right\|_{2,1} + \left\|\mathbf{G}^{(i)}\right\|_{1,2}\Big) + \gamma\left\|\boldsymbol{\mathcal{G}}\right\|_1$$
$$\text{s.t. } \boldsymbol{\mathcal{T}} = \boldsymbol{\mathcal{G}} \times_1 \mathbf{A} \times_2 \mathbf{B} \times_3 \mathbf{C} + \boldsymbol{\mathcal{N}}, \boldsymbol{\mathcal{G}} \in \mathbb{R}^{R_1^{est}\times R_2^{est}\times R_3^{est}},$$
$$\mathbf{A} \in \mathbb{R}^{I_1\times R_1^{est}}, \mathbf{B} \in \mathbb{R}^{I_2\times R_2^{est}}, \mathbf{C} \in \mathbb{R}^{I_3\times R_3^{est}} \quad (18)$$

Obviously, it is not necessary to consider sparse constraints anymore, so the weighting parameters are set to zero, i.e. $\lambda_1 = \lambda_2 = \lambda_3 = \gamma = 0$. The optimization procedure described in the section 4.1.1 is then used to estimate $\mathbf{A}$, $\mathbf{B}$ and $\mathbf{C}$.

4.1.3 Computation complexity analysis

The numerical complexity of R-MTD is the sum of the complexities of both steps described above. The computational complexity required to estimate the loading matrices is basically the same of the complexity of the rank estimation step. Therefore, we focus on the later. The complexity is analyzed in terms of number of multiplications. Note that we use the $\mathbf{LDL}^\intercal$ decomposition to compute the symmetrical matrix inverse in order to reduce the complexity. The computational complexity of R-MTD depends on the initialized sizes of $\widehat{\boldsymbol{\mathcal{G}}}$ and $\boldsymbol{\mathcal{T}}$. The formulas (5), (6) and (7) involve Kronecker products and matrix inverses. These Kronecker products require $I_1I_2I_3(\widehat{R}_1+\widehat{R}_2+\widehat{R}_3)+I_2I_3(\widehat{R}_2\widehat{R}_3+\widehat{R}_2^2\widehat{R}_3^2+\widehat{R}_1\widehat{R}_2\widehat{R}_3)+I_1I_3(\widehat{R}_1\widehat{R}_3+\widehat{R}_1^2\widehat{R}_3^2+\widehat{R}_1\widehat{R}_2\widehat{R}_3)+I_1I_2(\widehat{R}_1\widehat{R}_2+\widehat{R}_1^2\widehat{R}_2^2+\widehat{R}_1\widehat{R}_2\widehat{R}_3)+I_1\widehat{R}_1^2+I_2\widehat{R}_2^2+I_3\widehat{R}_3^2$ multiplications. The computation of the matrix inverses need $\frac{\widehat{R}_1^3\widehat{R}_2^3\widehat{R}_3^3}{2} + 9\widehat{R}_1^2\widehat{R}_2^2\widehat{R}_3^2 + \frac{5}{2}\widehat{R}_1\widehat{R}_2\widehat{R}_3$ products. The computational complexity of (8), (9) and (10) is $(\widehat{R}_1\widehat{R}_2\widehat{R}_3 + \widehat{R}_2\widehat{R}_3)I_2I_3 + (\widehat{R}_1\widehat{R}_2\widehat{R}_3 + \widehat{R}_1\widehat{R}_3)I_1I_3 + (\widehat{R}_1\widehat{R}_2\widehat{R}_3 + \widehat{R}_1\widehat{R}_2)I_1I_2 + \widehat{R}_1(I_1 + I_1I_2I_3) + \widehat{R}_2(I_2 + I_1I_2I_3) + \widehat{R}_3(I_3 + I_1I_2I_3) + \widehat{R}_1^2(I_1 + 7I_2I_3) + \widehat{R}_2^2(I_2 + 7I_1I_3) + \widehat{R}_3^2(I_3 + 7I_1I_2) + \frac{11}{3}(\widehat{R}_1^3 + \widehat{R}_2^3 + \widehat{R}_3^3)$. The number of multiplications required by the SVD in (17) is $7\widehat{R}_1\widehat{R}_2\widehat{R}_3(\widehat{R}_1^2 + \widehat{R}_2^2 + \widehat{R}_3^2) + \frac{11}{3}(\widehat{R}_1^3 + \widehat{R}_2^3 + \widehat{R}_3^3)$. Therefore, the total of multiplications needed by R-OMTD is $2I_1I_2I_3(\widehat{R}_1 + \widehat{R}_2 + \widehat{R}_3) + I_2I_3(2\widehat{R}_2\widehat{R}_3 + \widehat{R}_2^2\widehat{R}_3^2 + 2\widehat{R}_1\widehat{R}_2\widehat{R}_3 + 7\widehat{R}_1^2) + I_1I_3(2\widehat{R}_1\widehat{R}_3 + \widehat{R}_1^2\widehat{R}_3^2 + 2\widehat{R}_1\widehat{R}_2\widehat{R}_3 + 7\widehat{R}_2^2) + I_1I_2(2\widehat{R}_1\widehat{R}_2 + \widehat{R}_1^2\widehat{R}_2^2 + 2\widehat{R}_1\widehat{R}_2\widehat{R}_3 + 7\widehat{R}_3^2) + I_1(\widehat{R}_1 + 2\widehat{R}_1^2) + I_2(\widehat{R}_2 + 2\widehat{R}_2^2) + I_3(\widehat{R}_3 + 2\widehat{R}_3^2) + \frac{\widehat{R}_1^3\widehat{R}_2^3\widehat{R}_3^3}{2} + 7\widehat{R}_1\widehat{R}_2\widehat{R}_3(\widehat{R}_1^2 + \widehat{R}_2^2 + \widehat{R}_3^2) + 9\widehat{R}_1^2\widehat{R}_2^2\widehat{R}_3^2 + \frac{5}{2}\widehat{R}_1\widehat{R}_2\widehat{R}_3 + \frac{22}{3}(\widehat{R}_1^3 + \widehat{R}_2^3 + \widehat{R}_3^3)$. By assuming that $I_1 = I_2 = I_3 = I$ and $\widehat{R}_1 = \widehat{R}_2 = \widehat{R}_3 = \widehat{R}$, the numerical complexity of R-MTD is $\mathcal{O}(I^3\widehat{R} + \widehat{R}^9)$.

4.2 R-OMTD method

Based on the analysis of the computational complexity of R-MTD, it appears that the latter method cannot be applied to large scale tensors. Another hard point is the huge physical memory required for the matrix Kronecker product, such as $\left[\left(\widehat{\mathbf{B}}_k \otimes \widehat{\mathbf{C}}_k\right)^\intercal\left(\widehat{\mathbf{B}}_k \otimes \widehat{\mathbf{C}}_k\right)\right] \otimes \left(u\widehat{\mathbf{A}}_k^\intercal\widehat{\mathbf{A}}_k\right)$. In order to process big data, we should improve the R-MTD method imposing an orthonormal constraint on loading matrices for a more efficient computation as HOOI [13]. Then the computational complexity of the numerous Kronecker products and matrix inverse operations will be neglected because of the orthogonality property. The more efficient resulting method is called R-OMTD (R-Orthonormal MTD).

4.2.1 R-OMTD for rank estimation

The minimization problem solved by R-OMTD is given by:

$$\min_{\widehat{\mathbf{A}},\widehat{\mathbf{B}},\widehat{\mathbf{C}},\widehat{\boldsymbol{\mathcal{G}}}} \sum_{i=1}^{3}\lambda_i\Big(\left\|\widehat{\mathbf{G}}^{(i)}\right\|_{2,1} + \left\|\widehat{\mathbf{G}}^{(i)}\right\|_{1,2}\Big) + \left\|\widehat{\boldsymbol{\mathcal{G}}}\right\|_1$$
$$\text{s.t. } \boldsymbol{\mathcal{T}} = \widehat{\boldsymbol{\mathcal{G}}} \times_1 \widehat{\mathbf{A}} \times_2 \widehat{\mathbf{B}} \times_3 \widehat{\mathbf{C}}, \widehat{\boldsymbol{\mathcal{G}}} \in \mathbb{R}^{\widehat{R}_1\times\widehat{R}_2\times\widehat{R}_3},$$
$$\widehat{\mathbf{A}}^\intercal\widehat{\mathbf{A}} = \mathbf{I},\ \widehat{\mathbf{B}}^\intercal\widehat{\mathbf{B}} = \mathbf{I},\ \widehat{\mathbf{C}}^\intercal\widehat{\mathbf{C}} = \mathbf{I},$$
$$\widehat{\mathbf{A}} \in \mathbb{R}^{I_1\times\widehat{R}_1}, \widehat{\mathbf{B}} \in \mathbb{R}^{I_2\times\widehat{R}_2}, \widehat{\mathbf{C}} \in \mathbb{R}^{I_3\times\widehat{R}_3} \quad (19)$$

The associated augmented Lagrangian function $\mathcal{L}$ depending on variables $(\widehat{\boldsymbol{\mathcal{G}}}, \widehat{\mathbf{A}}, \widehat{\mathbf{B}}, \widehat{\mathbf{C}}, \widehat{\boldsymbol{\mathcal{P}}}, \widehat{\boldsymbol{\mathcal{Y}}}, \beta, \boldsymbol{\Phi}^{(i)}, \boldsymbol{\Psi}^{(i)})$ is defined by:

$$\mathcal{L} = \sum_{i=1}^{3}\lambda_i\Big[Tr\big(\widehat{\mathbf{G}}^{(i)^\intercal}\boldsymbol{\Phi}^{(i)}\widehat{\mathbf{G}}^{(i)}\big) + Tr\big(\widehat{\mathbf{G}}^{(i)}\boldsymbol{\Psi}^{(i)}\widehat{\mathbf{G}}^{(i)^\intercal}\big)\Big] + \left\|\widehat{\boldsymbol{\mathcal{P}}}\right\|_1 + \frac{u}{2}\left\|\boldsymbol{\mathcal{T}} - \widehat{\boldsymbol{\mathcal{G}}} \times_1 \widehat{\mathbf{A}} \times_2 \widehat{\mathbf{B}} \times_3 \widehat{\mathbf{C}}\right\|_F^2 + \left\langle\widehat{\boldsymbol{\mathcal{G}}} - \widehat{\boldsymbol{\mathcal{P}}}, \widehat{\boldsymbol{\mathcal{Y}}}\right\rangle + \frac{\beta}{2}\left\|\widehat{\boldsymbol{\mathcal{G}}} - \widehat{\boldsymbol{\mathcal{P}}}\right\|_F^2, \text{ with } \widehat{\mathbf{A}}^\intercal\widehat{\mathbf{A}} = \mathbf{I}, \widehat{\mathbf{B}}^\intercal\widehat{\mathbf{B}} = \mathbf{I}, \widehat{\mathbf{C}}^\intercal\widehat{\mathbf{C}} = \mathbf{I} \quad (20)$$

For the sake of simplicity, we directly give the update rule of $\widehat{\mathbf{G}}^{(1)}$:

$$\text{vec}(\widehat{\mathbf{G}}_{k+1}^{(1)}) = \Big\{\mathbf{I} \otimes \left(2\lambda_1\boldsymbol{\Phi}_k^{(1)}\right) + \left(2\lambda_1\boldsymbol{\Psi}_k^{(1)} + \beta_k\mathbf{I}\right) \otimes \mathbf{I} + \left[\left(\widehat{\mathbf{B}}_k \otimes \widehat{\mathbf{C}}_k\right)^\intercal\left(\widehat{\mathbf{B}}_k \otimes \widehat{\mathbf{C}}_k\right)\right] \otimes \left(u\widehat{\mathbf{A}}_k^\intercal\widehat{\mathbf{A}}_k\right)\Big\}^{-1} \text{vec}\Big[\beta_k\widehat{\mathbf{P}}_k^{(1)} - \widehat{\mathbf{Y}}_k^{(1)} + u\widehat{\mathbf{A}}_k^\intercal\mathbf{T}^{(1)}\left(\widehat{\mathbf{B}}_k \otimes \widehat{\mathbf{C}}_k\right)\Big] \quad (21)$$

By using $\big(\widehat{\mathbf{B}}_k \otimes \widehat{\mathbf{C}}_k\big)^\intercal \big(\widehat{\mathbf{B}}_k \otimes \widehat{\mathbf{C}}_k\big) = \mathbf{I}$ and $u\widehat{\mathbf{A}}_k^\intercal \widehat{\mathbf{A}}_k = u\mathbf{I}$, the equation (21) can be simplified as follows:

$$\operatorname{vec}(\widehat{\mathbf{G}}_{k+1}^{(1)}) = \Big\{\mathbf{I} \otimes \big(2\lambda_1 \mathbf{\Phi}_k^{(1)}\big) + \big(2\lambda_1 \mathbf{\Psi}_k^{(1)} + \beta_k \mathbf{I} + u\mathbf{I}\big) \otimes \mathbf{I}\Big\}^{-1} \operatorname{vec}\Big[\beta_k \widehat{\mathbf{P}}_k^{(1)} - \widehat{\mathbf{Y}}_k^{(1)} + u\widehat{\mathbf{A}}_k^\intercal \mathbf{T}^{(1)}\big(\widehat{\mathbf{B}}_k \otimes \widehat{\mathbf{C}}_k\big)\Big] \tag{22}$$

The update rules of $\widehat{\mathbf{G}}^{(2)}$ and $\widehat{\mathbf{G}}^{(3)}$ are given by:

$$\operatorname{vec}(\widehat{\mathbf{G}}_{k+1}^{(2)}) = \Big\{\mathbf{I} \otimes \big(2\lambda_2 \mathbf{\Phi}_k^{(2)}\big) + \big(2\lambda_2 \mathbf{\Psi}_k^{(2)} + \beta_k \mathbf{I} + u\mathbf{I}\big) \otimes \mathbf{I}\Big\}^{-1} \operatorname{vec}\Big[\beta_k \widehat{\mathbf{P}}_k^{(2)} - \widehat{\mathbf{Y}}_k^{(2)} + u\widehat{\mathbf{B}}_k^\intercal \mathbf{T}^{(2)}\big(\widehat{\mathbf{C}}_k \otimes \widehat{\mathbf{A}}_k\big)\Big] \tag{23}$$

and:

$$\operatorname{vec}(\widehat{\mathbf{G}}_{k+1}^{(3)}) = \Big\{\mathbf{I} \otimes \big(2\lambda_3 \mathbf{\Phi}_k^{(3)}\big) + \big(2\lambda_3 \mathbf{\Psi}_k^{(3)} + \beta_k \mathbf{I} + u\mathbf{I}\big) \otimes \mathbf{I}\Big\}^{-1} \operatorname{vec}\Big[\beta_k \widehat{\mathbf{P}}_k^{(3)} - \widehat{\mathbf{Y}}_k^{(3)} + u\widehat{\mathbf{C}}_k^\intercal \mathbf{T}^{(3)}\big(\widehat{\mathbf{A}}_k \otimes \widehat{\mathbf{B}}_k\big)\Big] \tag{24}$$

respectively. The updating rules of $\big(\mathbf{\Phi}_k^{(1)}, \mathbf{\Psi}_k^{(1)}\big)$, $\big(\mathbf{\Phi}_k^{(2)}, \mathbf{\Psi}_k^{(2)}\big)$ and $\big(\mathbf{\Phi}_k^{(3)}, \mathbf{\Psi}_k^{(3)}\big)$ are same with the descriptions in section 4.1.1.

Then the orthonormal loading matrix $\widehat{\mathbf{A}}$ is updated by solving the following sub-problem:

$$\min_{\widehat{\mathbf{A}}} \ \big\|\mathbf{T}^{(1)} - \widehat{\mathbf{A}}\widehat{\mathbf{G}}_{k+1}^{(1)}\big(\widehat{\mathbf{B}}_k \otimes \widehat{\mathbf{C}}_k\big)^\intercal\big\|_F^2 \quad \text{with} \quad \widehat{\mathbf{A}}^\intercal\widehat{\mathbf{A}} = \mathbf{I} \tag{25}$$

The closed-form solution of $\widehat{\mathbf{A}}_{k+1}$ in (25) has been proved and discussed in [56], [5], [33]. It is given by:

$$\widehat{\mathbf{A}}_{k+1} = \mathbf{U}^{(1)}\mathbf{V}^{(1)^\intercal} \tag{26}$$

where $\mathbf{U}^{(1)}$ and $\mathbf{V}^{(1)}$ are the orthonormal matrices of the SVD of the matrix $\mathbf{H}_1$ given by $\mathbf{H}_1 = \mathbf{T}^{(1)}\big(\widehat{\mathbf{B}}_k \otimes \widehat{\mathbf{C}}_k\big)\widehat{\mathbf{G}}_{k+1}^{(1)^\intercal}$. Identically, $\widehat{\mathbf{B}}_{k+1}$ and $\widehat{\mathbf{C}}_{k+1}$ are computed as follows:

$$\widehat{\mathbf{B}}_{k+1} = \mathbf{U}^{(2)}\mathbf{V}^{(2)^\intercal}, \ \ \widehat{\mathbf{C}}_{k+1} = \mathbf{U}^{(3)}\mathbf{V}^{(3)^\intercal} \tag{27}$$

where $(\mathbf{U}^{(2)}, \mathbf{V}^{(2)})$, $(\mathbf{U}^{(3)}, \mathbf{V}^{(3)})$ are derived from the SVD of $\mathbf{H}_2 = \mathbf{T}^{(2)}\big(\widehat{\mathbf{C}}_k \otimes \widehat{\mathbf{A}}_{k+1}\big)\widehat{\mathbf{G}}_{k+1}^{(2)^\intercal}$ and $\mathbf{H}_3 = \mathbf{T}^{(3)}\big(\widehat{\mathbf{A}}_{k+1} \otimes \widehat{\mathbf{B}}_{k+1}\big)\widehat{\mathbf{G}}_{k+1}^{(3)^\intercal}$, respectively.

The update rules of $\widehat{\boldsymbol{\mathcal{P}}}$, $\widehat{\boldsymbol{\mathcal{Y}}}$ and β are the same as those of the R-MTD method. The estimated rank R_i^{est} can be also estimated using the MDL approach of the unfolding matrix $\widehat{\mathbf{G}}_{k+1}^{(i)}$ as in (17).

4.2.2 R-OMTD for an estimation of the loading matrices

The estimated multilinear rank $(R_1^{est}, R_2^{est}, R_3^{est})$ is exploited in (19), leading to the following minimization problem:

$$\begin{aligned}\min_{\mathbf{A},\mathbf{B},\mathbf{C},\boldsymbol{\mathcal{G}}} \ & \sum_{i=1}^{3} \lambda_i\Big(\big\|\mathbf{G}^{(i)}\big\|_{2,1} + \big\|\mathbf{G}^{(i)}\big\|_{1,2}\Big) + \gamma\|\boldsymbol{\mathcal{G}}\|_1 \\ \text{s.t.} \ & \boldsymbol{\mathcal{T}} = \boldsymbol{\mathcal{G}} \times_1 \mathbf{A} \times_2 \mathbf{B} \times_3 \mathbf{C} + \boldsymbol{\mathcal{N}}, \boldsymbol{\mathcal{G}} \in \mathbb{R}^{R_1^{est} \times R_2^{est} \times R_3^{est}}, \\ & \mathbf{A}^\intercal\mathbf{A} = \mathbf{I}, \ \ \mathbf{B}^\intercal\mathbf{B} = \mathbf{I}, \ \ \mathbf{C}^\intercal\mathbf{C} = \mathbf{I}, \\ & \mathbf{A} \in \mathbb{R}^{I_1 \times R_1^{est}}, \mathbf{B} \in \mathbb{R}^{I_2 \times R_2^{est}}, \mathbf{C} \in \mathbb{R}^{I_3 \times R_3^{est}}\end{aligned} \tag{28}$$

As for R-MTD method, it is not essential to consider sparse constraints anymore, so the weighting parameters are also set to zero, i.e. $\lambda_1 = \lambda_2 = \lambda_3 = \gamma = 0$. Then the optimization procedure described in the section 4.2.1 is used to estimate the loading matrices.

4.2.3 Computation complexity analysis

The computational complexity of (22), (23) and (24) is lower than the computational complexity of (5), (6) and (7) because of the fewer multiplications required for the computation of Kronecker products and the inverse of diagonal matrices. The computation of the Kronecker products of (22), (23) and (24) need $I_1I_2I_3(\widehat{R}_1 + \widehat{R}_2 + \widehat{R}_3) + I_2I_3(\widehat{R}_1\widehat{R}_2\widehat{R}_3 + \widehat{R}_2\widehat{R}_3) + I_1I_3(\widehat{R}_1\widehat{R}_2\widehat{R}_3 + \widehat{R}_1\widehat{R}_3) + I_1I_2(\widehat{R}_1\widehat{R}_2\widehat{R}_3 + \widehat{R}_1\widehat{R}_2)$ multiplications. The computation of the matrix inverses require only $3\widehat{R}_1\widehat{R}_2\widehat{R}_3$ multiplications. The number of multiplications required to compute (26) and (27) is $(\widehat{R}_1\widehat{R}_2\widehat{R}_3 + \widehat{R}_2\widehat{R}_3)I_2I_3 + (\widehat{R}_1\widehat{R}_2\widehat{R}_3 + \widehat{R}_1\widehat{R}_3)I_1I_3 + (\widehat{R}_1\widehat{R}_2\widehat{R}_3 + \widehat{R}_1\widehat{R}_2)I_1I_2 + (\widehat{R}_1 + \widehat{R}_2 + \widehat{R}_3)I_1I_2I_3 + 8I_1\widehat{R}_1^2 + 8I_2\widehat{R}_2^2 + 8I_3\widehat{R}_3^2 + \frac{11}{3}(\widehat{R}_1^3 + \widehat{R}_2^3 + \widehat{R}_3^3)$. On the other hand, R-OMTD also needs $7\widehat{R}_1\widehat{R}_2\widehat{R}_3(\widehat{R}_1^2 + \widehat{R}_2^2 + \widehat{R}_3^2) + \frac{11}{3}(\widehat{R}_1^3 + \widehat{R}_2^3 + \widehat{R}_3^3)$ multiplications to compute the SVD in (17). Hence, the total number of multiplications required by R-OMTD is $2I_1I_2I_3(\widehat{R}_1 + \widehat{R}_2 + \widehat{R}_3) + 2I_2I_3(\widehat{R}_2\widehat{R}_3 + \widehat{R}_1\widehat{R}_2\widehat{R}_3) + 2I_1I_3(\widehat{R}_1\widehat{R}_3 + \widehat{R}_1\widehat{R}_2\widehat{R}_3) + 2I_1I_2(\widehat{R}_1\widehat{R}_2 + \widehat{R}_1\widehat{R}_2\widehat{R}_3) + 8I_1\widehat{R}_1^2 + 8I_2\widehat{R}_2^2 + 8I_3\widehat{R}_3^2 + 7\widehat{R}_1\widehat{R}_2\widehat{R}_3(\widehat{R}_1^2 + \widehat{R}_2^2 + \widehat{R}_3^2) + 3\widehat{R}_1\widehat{R}_2\widehat{R}_3 + \frac{22}{3}(\widehat{R}_1^3 + \widehat{R}_2^3 + \widehat{R}_3^3)$. Similarly, by assuming that $I_1 = I_2 = I_3 = I$ and $\widehat{R}_1 = \widehat{R}_2 = \widehat{R}_3 = \widehat{R}$, the numerical complexity of R-MTD is $\mathcal{O}(I^3\widehat{R} + \widehat{R}^5)$. Besides, the fewer memory allocated to compute Kronecker products is avoided because of the diagonality/sparsity of the considered matrices.

4.3 Convergence analysis

Regarding the minimization problems solved by the R-MTD and R-OMTD methods, it is straightforward that all the sub-problems have a closed-form solution, so the proposed methods will find an approximate solution after k iterations and the convergence rate is $\mathcal{O}(1/k)$ based on the result proved in [57].

5 Results

In this section we firstly evaluated the performance of R-MTD and R-OMTD methods on rank estimation and signal denoising using noisy simulated data. Then, noiseless Amino Acids Fluorescence data[1] [58] were exploited to test the rank estimation accuracy of the proposed methods on real data. Besides, a convergence study of R-MTD and R-OMTD was made. Eventually, the behavior of the R-OMTD algorithm on signal denoising was investigated using the noisy MultiSpectral Image (MSI) data (Columbia MSI database[2] [59] and Urban MSI data[3]). For each experiment, a comparative study with the recent published SCORE[4] [28] and KBR[5] [33] methods, which are more efficient than the state-of-the-art methods, was also provided.

5.1 Simulated data experiments

Simulated data generation We first generated the multilinear tensor $\boldsymbol{\mathcal{F}} = \boldsymbol{\mathcal{G}} \times_1 \mathbf{A} \times_2 \mathbf{B} \times_3 \mathbf{C}$ (Fig. 2 (a)), with $I_1 = I_2 = I_3 = 100$ and five different sizes of the core tensor such as $R_1 = R_2 = R_3 = 3$, $R_1 = R_2 = R_3 = 4$, $R_1 = R_2 = R_3 = 5$, $R_1 = R_2 = R_3 = 6$ and $R_1 = 3, R_2 = 4, R_3 = 5$. All the components of the loading matrices and the core tensor follow a Gaussian distribution. The size of the over-estimated core tensor was

1. http://www.models.life.ku.dk/amino_acid_fluo
2. http://www1.cs.columbia.edu/CAVE/databases/multispectral
3. http://www.tec.army.mil/Hypercube
4. https://sites.google.com/site/yokotatsuya/home/publication
5. http://gr.xjtu.edu.cn/web/dymeng.

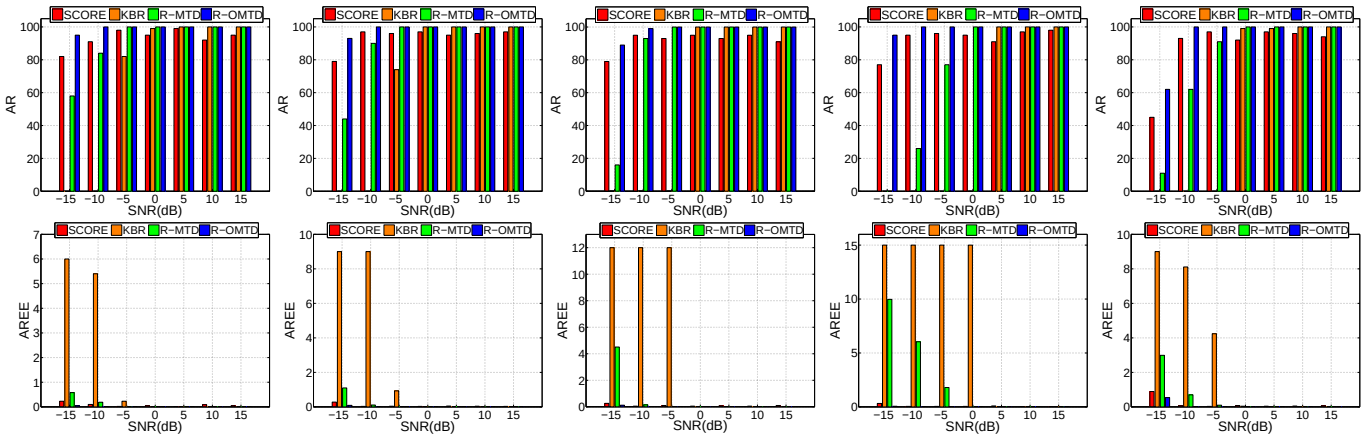

(a) $(3 \times 3 \times 3)$ (b) $(4 \times 4 \times 4)$ (c) $(5 \times 5 \times 5)$ (d) $(6 \times 6 \times 6)$ (e) $(3 \times 4 \times 5)$

Fig. 3: The Accuracy Rate (AR) and the Average Rank Estimation Error (AREE) criteria for different sizes of the core tensor as a function of SNR.

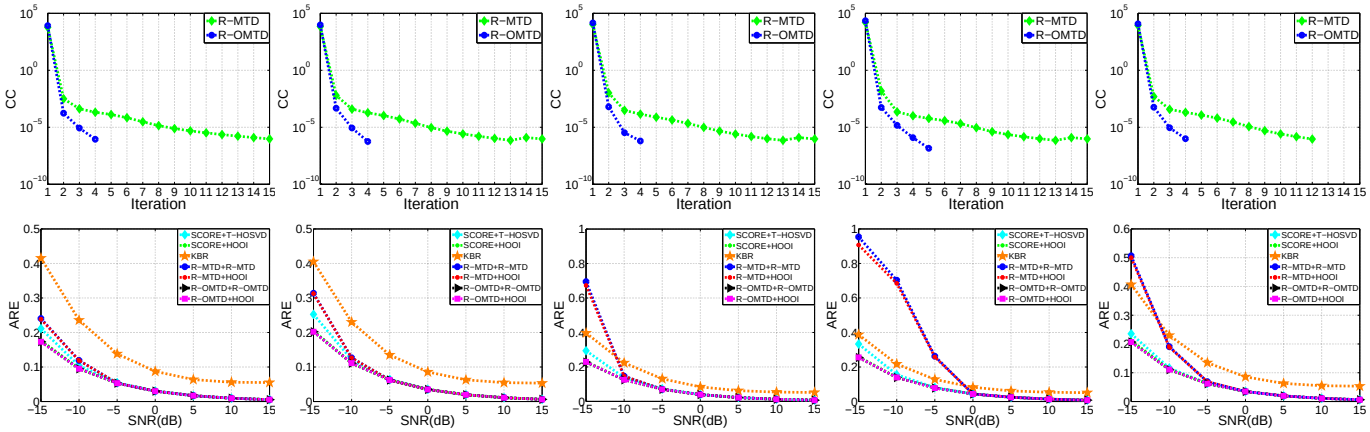

(a) $(3 \times 3 \times 3)$ (b) $(4 \times 4 \times 4)$ (c) $(5 \times 5 \times 5)$ (d) $(6 \times 6 \times 6)$ (e) $(3 \times 4 \times 5)$

Fig. 4: The Convergence Criterion (CC) for different sizes of the core tensor under SNR=0dB and the Average Relative Error (ARE) criterion for different sizes of the core tensor as a function of SNR.

fixed to $\widehat{R}_1 = \widehat{R}_2 = \widehat{R}_3 = 10$. In addition, the noise tensor $\boldsymbol{\mathcal{N}} \in \mathbb{R}^{I_1 \times I_2 \times I_3}$ also follows a Gaussian distribution with different SNR values. Finally, the noisy tensor $\boldsymbol{\mathcal{T}}$ was obtained as follows:

$$\boldsymbol{\mathcal{T}} = \boldsymbol{\mathcal{F}} + \sigma \frac{\|\boldsymbol{\mathcal{F}}\|_F}{\|\boldsymbol{\mathcal{N}}\|_F} \boldsymbol{\mathcal{N}},$$

where the parameter σ determines the SNR defined as $\text{SNR} = -20\log_{10}(\sigma)$. Different SNR values (-15dB to 15dB with a 5dB step size) were considered in this experiment and 100 independent Monte Carlo (MC) trials were run for each case.

Parameter setting The selection of the weighting parameter λ_i should be much larger when the size of the underlying core tensor is much smaller than the over-estimated core tensor size. In this experiment, the selected λ_i was set to: $\lambda_i = 5$ for $i = 1, 2, 3$. The other parameters μ, β, ρ and $tolerance$ were fixed to 0.01, 0.3, 20 and 1e-6.

Rank estimation performance Two criteria were designed to evaluate the performance of the methods on rank estimation. The first one is the Accuracy Rate (AR), which computes the successful times of the rank estimation and is defined as:

$$\text{AR} : \text{Times of } R_i = R_i^{est}, i = 1, 2, 3.$$

The second one is the Average Rank Estimation Error (AREE), which measures the deviation between the estimated rank and simulated rank, is defined as follows:

$$\text{AREE} : \frac{1}{100} \sum_{\text{times}=1}^{100} \Big(\sum_{i=1}^{3} |R_i - R_i^{est}| \Big).$$

The AR results obtained by R-MTD, R-OMTD, KBR and SCORE were depicted in Fig. 3 (first row), as a function of SNR, for different sizes of the core tensor. For SNR values from 0dB to 15dB, R-MTD and R-OMTD always succeeded in the estimation of the true rank, whatever the core tensor sizes. This is not the case of the SCORE method for which the success rate is about 90%. Obviously, the KBR method presents the worst performance, especially for smaller SNR values. In addition, we note that the AR results of KBR are decreased more dramatically compared with R-MTD as the size of the core tensor is increased from 3 to 6. In contrary, R-OMTD performance is more robust with respect to the size of the core tensor. The AR results for the last case, i.e. a core tensor of size $3 \times 4 \times 5$, demonstrate that these methods can be also applied for non-square core tensors. Note that the R-OMTD method outperforms the SCORE and KBR methods whatever the considered scenario is.

The second row of Fig. 3 shows the AREE results. We observe that the rank estimation error at the output of R-OMTD is the lowest for each scenario. This suggests that R-

OMTD is the most outstanding method for rank estimation (even if the SCORE method shows rather satisfactory results in terms of AREE).

Convergence testing The Convergence Criterion (CC) defined in equation (16) is a useful index to evaluate convergence. An example, for SNR=0dB, of CC values as a function of the number of iterations is displayed in the first row of Fig. 4 for both R-MTD and R-OMTD. For all the scenarios, the proposed methods converge after a small number of iterations. Furthermore, the convergence rate of R-OMTD is always better than that of R-MTD, concluding that the proposed R-OMTD method is more appropriate for large-scale data.

Signal denoising efficiency The denoising effectiveness of the proposed methods is assessed through the Average Relative Error (ARE) criterion defined as:

$$\text{ARE} : \frac{1}{100} \sum_{\text{times}=1}^{100} \frac{\|\boldsymbol{\mathcal{F}}^{est} - \boldsymbol{\mathcal{F}}\|_F}{\|\boldsymbol{\mathcal{F}}\|_F},$$

where $\boldsymbol{\mathcal{F}}^{est}$, $\boldsymbol{\mathcal{F}}$ are the estimated tensor and the true tensor, respectively. We consider different combinations of rank estimation methods and tensor decomposition algorithms, namely SCORE+T-HOSVD (Truncated-HOSVD), SCORE+HOOI, R-MTD+R-MTD, R-MTD+HOOI, R-OMTD+R-OMTD and R-OMTD+HOOI. The KBR method performing low-rank approximation and denoising simultaneously is also considered.

The second row of Fig. 4 presents the obtained ARE results at the output of the seven approaches, as a function of SNR, for different sizes of the core tensor. Clearly, R-OMTD+R-OMTD, R-OMTD+HOOI and SCORE+HOOI offer the best performance, especially for smaller SNR values. This is in agreement with the results obtained in Fig. 3 (row 2), which shows that the AREE criterion is still very small even if these methods do not always succeed in the estimation of the true rank. The ARE values given by R-MTD+R-MTD and R-MTD+HOOI (for small SNR values) are larger because of the high AREE value at the output of R-MTD (see row 2 in Fig.3). These results suggest that the robustness of R-OMTD with respect to noise for rank estimation is considerably increased using the orthonormality constraint.

Note also that, the ARE value at the output of SCORE+T-HOSVD is always smaller than the one given by SCORE+HOOI. In other words, the denoising effectiveness of HOOI is better than that of T-HOSVD. This can be explained by the fact that the T-HOSVD method only extracts the first R_i^{est} components without any denoising process. Therefore it cannot give excellent denoising results for small SNR values. Besides, the ARE results given by KBR are always larger than others for larger SNR values even if the rank estimated by KBR is exact (see Fig. 3). Indeed the KBR method always uses the over-estimated core tensor during the loading matrix estimation process. Furthermore, KBR gives similar ARE results for different sizes of the core tensor due to the use of the same size of the over-estimated core tensor.

5.2 Real data experiments

5.2.1 *Rank estimation using amino acids fluorescence data*

In this subsection, the efficiency of R-MTD and R-OMTD on real data is studied and compared to that of SCORE and KBR. To do so, amino acids fluorescence data which consist of five laboratory-made samples, are used. Each sample contains different amounts of tyrosine, tryptophan and phenylalanine dissolved in phosphate buffered water. The samples were measured by fluorescence (excitation 240-300 nm, emission 250-450 nm, 1 nm intervals) on a PE LS50B spectrofluorometer. The three-way array data to be decomposed is hence of size $5 \times 61 \times 201$. In this experiment, the parameters were fixed as follows: $\lambda_i = 5, i = 1, 2, 3$, $\mu = 0.1$, $\beta = 0.3$, $\rho = 20$ and $tolerance = 1e-6$. The three methods were initialized using an over-estimated core tensor of size $5 \times 5 \times 5$.

The MDL criterion (see equation (17)) obtained for SCORE, KBR, R-MTD and R-OMTD methods is displayed in Fig. 5. The position of the lowest point is indicated by the red circle and the related X-axis index gives the rank esti-

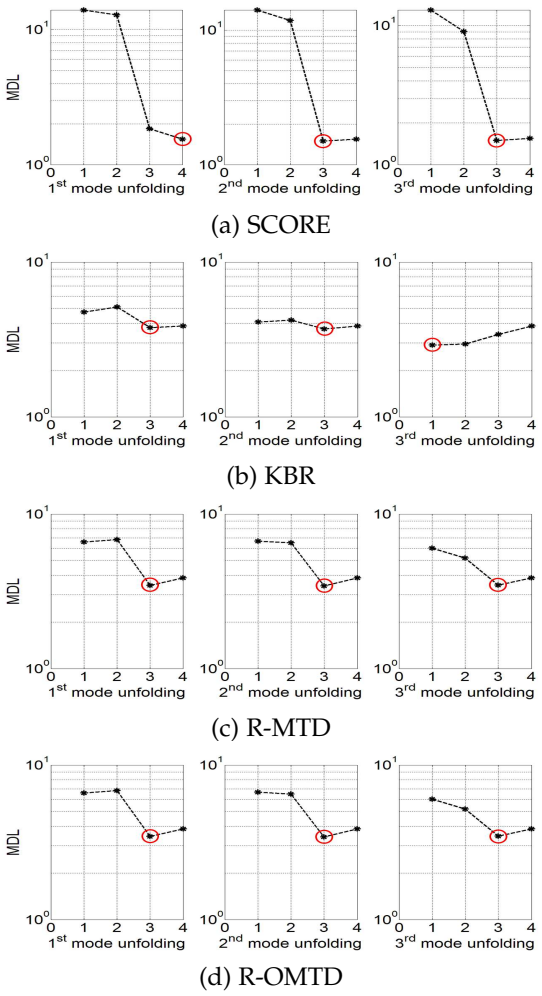

(a) SCORE

(b) KBR

(c) R-MTD

(d) R-OMTD

Fig. 5: Amino acids fluorescence data: the MDL criterion at the output of the unfolding matrices.

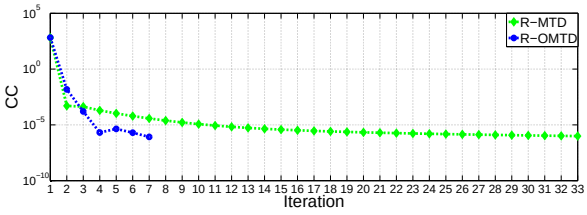

Fig. 6: Amino acids fluorescence data: the Convergence Criterion (CC) of the proposed methods.

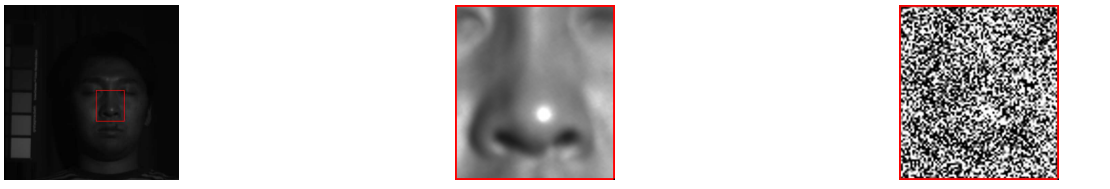

Original image (a) Clean image (b) Noisy image

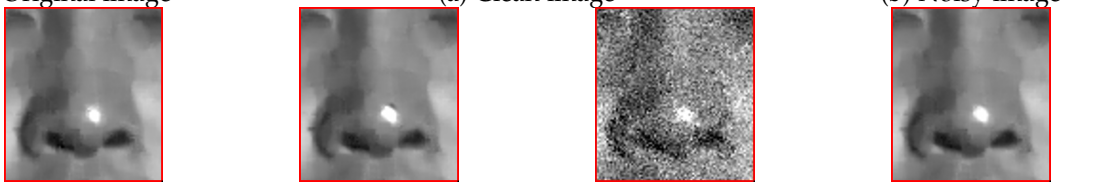

(c) SCORE+T-HOSVD (d) SCORE+HOOI (e) KBR (f) R-OMTD+R-OMTD

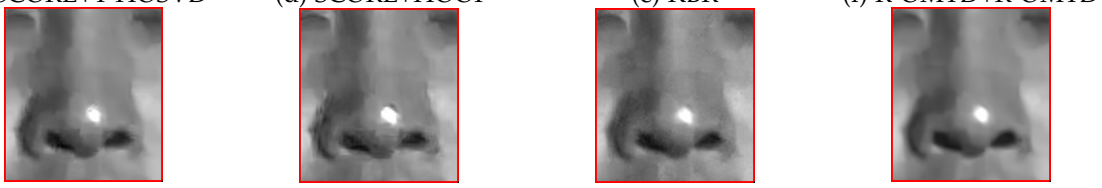

(g) SCORE+T-HOSVD (h) SCORE+HOOI (i) KBR (j) R-OMTD+R-OMTD

Fig. 7: Columbia MSI data: (a) The amplified image of the first band (400nm) of face; (b) The amplified noisy image with variance $v = 0.2$; (c)-(f) The amplified images of the recovered results by the first time denoising; (g)-(j) The reconstructed images after 2 times denoising process.

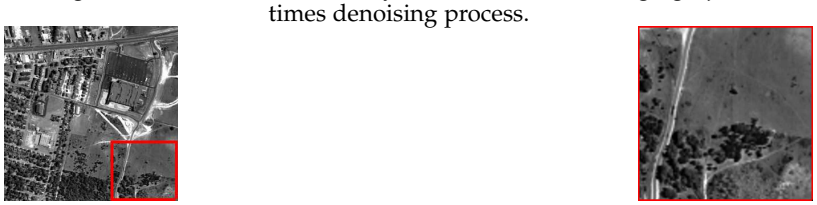

Original Image (a) Original Image

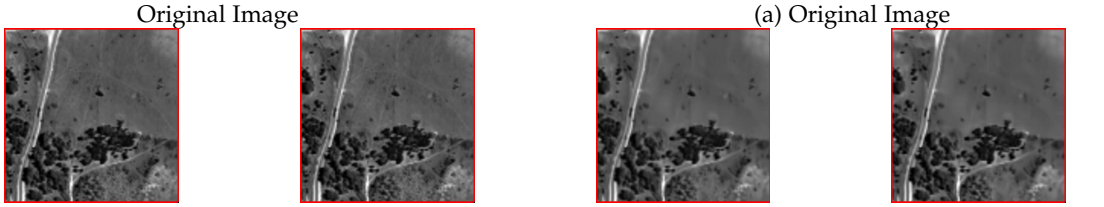

(b) SCORE+T-HOSVD (c) SCORE+HOOI (d) KBR (e) R-OMTD+R-OMTD

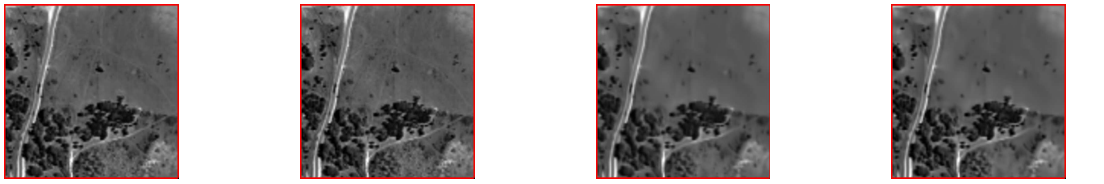

(f) SCORE+T-HOSVD (g) SCORE+HOOI (h) KBR (i) R-OMTD+R-OMTD

Fig. 8: Urban MSI data: (a) The magnifying image (red square) of the 100th band (1400nm) of the urban MSI; (b)-(e) The amplified images of the denoising results after the first denoising process; (f)-(i) The magnifying image of the restored images after the second denoising.

mated by each method. The estimated rank values given by SCORE and KBR are $(4, 3, 3)$ and $(3, 3, 1)$ according to Fig. 5 (a) and (b), which are close to the true rank. The proposed methods give the almost same MDL curves and provide an accurate estimated rank value $(3, 3, 3)$, as shown in Fig. 5 (c) and (d). We also assess the good convergence behavior of the proposed methods (see Fig. 6). The convergence rate of R-OMTD is still better than the convergence rate of R-MTD (the CC can be satisfied after 33 iterations for R-MTD while only 7 iterations are required for R-OMTD). This result is in accordance with the one obtained on the simulated data.

5.2.2 MultiSpectral Image data denoising: Columbia MSI database

In this experiment, the R-MTD method appeared to be very time-consuming. Consequently only the proposed R-OMTD method was evaluated. The Columbia MSI Database [59] was used to perform this evaluation. This database consists of 32 scenes and each scene has a spatial resolution of 512×512 and a spectral resolution of 31, which includes reflectance data from 400nm to 700nm at 10nm steps. Each MSI is normalized and two kinds of Gaussian noise with different variance v ($v = 0.1$ and 0.2) are considered. We also adopt the nonlocal block matching technique to pre-

process the noisy MSI image as the flowchart of [33, Fig.5]. Applying block matching to Full Band Patches (FBP) of size 6×6 and choosing the first 50 similar groups, we build numerous FBP groups of size $36 \times 31 \times 50$. Then, we apply the proposed methods to each FBP group. After that, we can reconstruct the recovered MSI image using all the recovered FBP groups. The above process is implemented twice for a better restored result. More precisely, R-OMTD+R-OMTD is tested and compared to SCORE+T-HOSVD, SCORE+HOOI and KBR. The size of the over-estimated core tensor is $36 \times 31 \times 50$. Considering different variance cases, we adopt different parameter settings: i) for $v = 0.1$, the coefficients $\lambda_i = 0.5$ $(i = 1, 2, 3)$ were used first and the values $\lambda_i = 0.01$ $(i = 1, 2, 3)$ were used next. The other parameters μ, β, ρ and $tolerance$ were set to 0.001, 3, 20 and 1e-6, respectively. ii) for $v = 0.2$, the coefficients $\lambda_i = 1.5$ $(i = 1, 2, 3)$ were exploited first and the values $\lambda_i = 1$ $(i = 1, 2, 3)$ were used next. The other parameters were selected as for $v = 0.1$.

Fig. 7 presents an example of the face image denoising in the case of the noise variance $v = 0.2$. After one denoising (see the second row of Fig. 7), the reconstructed face image results given by SCORE and R-OMTD are more clean than those given by KBR. The obtained images are more clean after two denoising steps (see the third row of Fig. 7), whatever the used methods are. However, by observing the textures near the nostrils, it seems that the R-OMTD result is still the most outstanding among all the results. This is confirmed in Table 1 where conventional picture quality indices [60], namely the Peak Signal-to-Noise Ratio (PSNR) and the Structure SIMilarity (SSIM) criteria were computed on all the selected Columbia MSI images under different variances, for each method. The values of PSNR and SSIM, which must be much higher in the case of a good reconstruction quality, indicate that R-OMTD outperforms other methods in almost all the cases (about 91% of cases).

5.2.3 MultiSpectral Image data denoising: Urban MSI database

We still consider the methods adopted in the Columbia MSI experiments in this subsection. The Urban MSI as a natural scene is deserved to be tested here and the objective is to remove the real noise which has an unknown power because of the effect of atmosphere and water absorption. The size of the Urban MSI, which has 210 wavelengths ranging from 400 nm to 2500 nm with a 10 nm spectral resolution, is $307 \times 307 \times 210$. Due to the severe pollution of the atmosphere and water absorption, several bands (76, 110-115, 130-155 and 201-210 nm) should be deleted. So the final tested Urban MSI is of size $307 \times 307 \times 157$. The experimental setting is the same as the last experimental setting, so each FBP group of size $36 \times 157 \times 50$ is used in this experiment. To reduce the computation complexity, an over-estimated core tensor of size $36 \times 10 \times 50$ is considered. All the adopted coefficients and parameters are the same as these used for the case $v = 0.1$ in the Columbia MSI data experiment.

The second row of Fig. 8 illustrates the restored images by R-OMTD+R-OMTD, SCORE+T-HOSVD, SCORE+HOOI and KBR using the first denoising. The reconstructed images using SCORE are almost identical to the original image, which means SCORE method cannot provide an optimal rank estimation in the first denoising process. The reconstructed results given by KBR and R-OMTD can remove the majority of unexpected stripes and Gaussian noise without loss of the textures and structures after the first denoising. The image results obtained after two denoisings are shown in the third row of Fig. 8. The image results of SCORE cannot be improved as before. The stripes and Gaussian noise are almost completely removed by KBR and R-OMTD. However, we can find that the image result of KBR is more blurred than the R-OMTD result, which means that the display resolution of the restored image by R-OMTD is more nicer.

6 Conclusion

A novel approach for robust multilinear tensor decomposition is proposed in this paper. The algorithm called R-MTD jointly estimates the multilinear rank and the loading matrices. The latter is mainly based on group sparsity and global sparsity of the over-estimated core tensor by means of the mixed-norms and the l_1 norm, respectively. Details and essential theorems to obtain a robust implementation of R-MTD have been given and proved. Furthermore, a second method, named R-OMTD, which imposes an orthonormal constraint on each loading matrix, is also proposed. This method, which can be seen as an improved version of R-MTD, is more robust with respect to the presence of noise and much faster than R-MTD. Simulations on noisy tensors and applications to real tensor data have been presented. The results obtained so far, especially those of R-OMTD, are very promising and our methods were shown to outperform the state-of-the-art algorithms. The real data examples considered in this paper confirm that the good performance of R-MTD and R-OMTD, which has been observed in the simulations, also holds for real data. Future work will consist in further consolidating the performance analysis of the R-MTD and R-OMTD algorithms by applying them in many other tensor applications, such as, tensor completion, tensor robust principal component analysis and biomedical tensor decomposition.

Appendix A

Proof. First, let's consider the square matrix case, i.e., $\mathbf{X} \in \mathbb{R}^{m \times n}$ with $m = n$. The SVD of $\mathbf{X}$ is given by $\mathbf{X} = \mathbf{U}\mathbf{S}\mathbf{V}^\intercal$ where $\mathbf{U} \in \mathbb{R}^{m \times m}$ and $\mathbf{V} \in \mathbb{R}^{m \times m}$ are orthonormal matrices and where the diagonal matrix $\mathbf{S} \in \mathbb{R}^{m \times m}$ contains the m singular values $s_k (1 \leq k \leq m)$. The relationship between $\mathbf{U}$ and $\mathbf{D}$ is given by $\mathbf{U} = \mathbf{D}\mathbf{\Omega}$, where $\mathbf{\Omega} \in \mathbb{R}^{m \times m}$ is an orthonormal rotation matrix. Consequently, we have $\|\boldsymbol{\alpha}\|_{2,1} = \|\mathbf{\Omega}\mathbf{S}\mathbf{V}^\intercal\|_{2,1}$. Let's consider that $\|\boldsymbol{\alpha}\|_{2,1} = f(s_1, s_2, \ldots, s_m)$ and $\|\mathbf{X}\|_* = g(s_1, s_2, \ldots, s_m)$, where f and g are two nonnegative functions of $\mathbb{R}^m$. Let's define $\mathcal{S}$ as the set of the points $\mathbf{s} = (s_1, s_2, \ldots, s_m) \in \mathbb{R}^m$ such that $s_1 \geq s_2 \geq \cdots \geq s_m$. The proof consists in exploring all the points of $\mathcal{S}$ by taking a particular road and by showing sequentially that the inequality $f \geq g$ holds for all the points of the road.

(i). We start the space exploration from the points $\mathbf{s} \in \mathcal{S}^{(1)}$ with $\mathcal{S}^{(1)} = \{\mathbf{s} \in \mathcal{S}, s_1 = s_2 = \cdots = s_m\}$. For these points we have:

$$f(\mathbf{s}) = \|\mathbf{\Omega S V}^\intercal\|_{2,1} = \sum_{i=1}^{m} \sqrt{\sum_{k=1}^{m} \Big(\sum_{j=1}^{m} \Omega_{i,j} s_j V_{k,j} \Big)^2} =$$

$$\sum_{i=1}^{m} \sqrt{\sum_{j=1}^{m}\sum_{k=1}^{m} \Big[\sum_{p=1,p\neq j}^{m} \big(2\Omega_{i,j} s_j V_{k,j} \Omega_{i,p} s_p V_{k,p}\big) + \big(\Omega_{i,j} s_j V_{k,j}\big)^2 \Big]}$$

Due to the orthonormal unit property of matrix $\mathbf{V}$, then $\sum_{j=1}^{m}\sum_{p=1,p\neq j}^{m}\sum_{k=1}^{m} \big(\Omega_{i,j} s_j V_{k,j} \Omega_{i,p} s_p V_{k,p}\big) = 0$ and $\sum_{j=1}^{m}\sum_{k=1}^{m} \big(\Omega_{i,j} s_j V_{k,j}\big)^2 = \sum_{j=1}^{m} \big(\Omega_{i,j} s_j\big)^2$. So we have:

$$f(\mathbf{s}) = \sum_{i=1}^{m} \sqrt{\sum_{j=1}^{m} \Omega_{i,j}^2 s_j^2} = \sum_{i=1}^{m} s \sqrt{\sum_{j=1}^{m} \Omega_{i,j}^2} = \sum_{j=1}^{m} s = g(\mathbf{s})$$

(ii). Now we continue the exploration of the space $\mathcal{S}$ from $\mathcal{S}^{(1)}$ by changing and increasing only the first $m-1$ components s_i such that $s_1 = s_2 = \cdots = s_{m-1} \geq s_m$. Let's define $\mathcal{S}^{(2)}$ as $\mathcal{S}^{(2)} = \{\mathbf{s} \in \mathcal{S}, s_1 = s_2 = \cdots = s_{m-1} \geq s_m\}$. Note that s_m does not change with respect to (i). Then we compute the first $m-1$ partial derivatives of f given by:

$$\begin{aligned}
&\frac{\partial f(\mathbf{s})}{\partial s_k} \\
&= \sum_{i=1}^{m} \frac{\Omega_{i,k}^2 s_k}{\sqrt{\sum_{j=1}^{k-1} \Omega_{i,j}^2 s_j^2 + \Omega_{i,k}^2 s_k^2 + \sum_{q=k+1}^{m-1} \Omega_{i,q}^2 s_q^2 + \Omega_{i,m}^2 s_m^2}} \\
&= \sum_{i=1}^{m} \frac{\Omega_{i,k}^2}{\sqrt{\sum_{j=1}^{m-1} \Omega_{i,j}^2 + \Omega_{i,m}^2 (s_m^2/s_k^2)}}, 1 \leq k \leq m-1
\end{aligned}$$

Since $s_m \leq s_k$ for $1 \leq k \leq m-1$ and $\sum_{j=1}^{m} \Omega_{i,j}^2 = 1$, we have $\sqrt{\sum_{j=1}^{m-1} \Omega_{i,j}^2 + \Omega_{i,m}^2 (s_m^2/s_k^2)} \leq 1$ and the following relationship:

$$\frac{\partial f(\mathbf{s})}{\partial s_k} \geq \sum_{i=1}^{m} \Omega_{i,k}^2 = 1 = \frac{\partial g(\mathbf{s})}{\partial s_k}$$

Thus, $f \geq g$ holds for every point $\mathbf{s}$ in $\mathcal{S}^{(2)}$.

Similarly, the exploration of the space $\mathcal{S}$ from $\mathcal{S}^{(t)}$ by changing and increasing the first $m-t$ components s_i such that $s_1 = s_2 = \cdots = s_{m-t} \geq \cdots \geq s_m$ is considered here. We define $\mathcal{S}^{(t+1)}$ as $\mathcal{S}^{(t+1)} = \{\mathbf{s} \in \mathcal{S}, s_1 = s_2 = \cdots = s_{m-t} \geq \cdots \geq s_m\}$. The partial derivative of f with respect to s_k, for $1 \leq k \leq m-t$, is computed as follows:

$$\frac{\partial f(\mathbf{s})}{\partial s_k} = \sum_{i=1}^{m} \frac{\Omega_{i,k}^2}{\sqrt{\sum_{j=1}^{m-t} \Omega_{i,j}^2 + \sum_{q=m-t+1}^{m} \Omega_{i,q}^2 (s_q^2/s_k^2)}}$$

Since $s_m \leq \ldots \leq s_{m-t+1} \leq s_k$ for $1 \leq k \leq m-t$ and $\sum_{j=1}^{m} \Omega_{i,j}^2 = 1$, we still have the following relationship:

$$\frac{\partial f(\mathbf{s})}{\partial s_k} \geq \sum_{i=1}^{m} \Omega_{i,k}^2 = 1 = \frac{\partial g(\mathbf{s})}{\partial s_k}$$

So $f \geq g$ still holds for each point $\mathbf{s}$ in $\mathcal{S}^{(t+1)}$.

In the same way, we can prove that $f \geq g$ holds in the following subspaces. From the above analysis, we derive that $\|\boldsymbol{\alpha}\|_{2,1} \geq \|\mathbf{X}\|_*$ for $m = n$.

Now let's consider the thin cases, i.e. $m > n$ and $m < n$. The issue for these two cases is not hard to derive after the transformation of the matrix $\mathbf{X}$ into a square matrix by filling with zero components. For the $m > n$ case, we use $\widehat{\mathbf{X}}$ as the transformation of $\mathbf{X}$, with $\widehat{\mathbf{X}} = [\mathbf{X}; \mathbf{0} \in \mathbb{R}^{m \times (m-n)}] \in \mathbb{R}^{m \times m}$. Obviously, the mixed-norm $\|\widehat{\boldsymbol{\alpha}}\|_{2,1}$ associated to $\widehat{\mathbf{X}}$ is the same as $\|\boldsymbol{\alpha}\|_{2,1}$, i.e. $\|\widehat{\boldsymbol{\alpha}}\|_{2,1} = \|\boldsymbol{\alpha}\|_{2,1}$, and the nuclear norm of $\widehat{\mathbf{X}}$ is also equal to that of $\mathbf{X}$, i.e. $\|\widehat{\mathbf{X}}\|_* = \|\mathbf{X}\|_*$. So we obtain $\|\boldsymbol{\alpha}\|_{2,1} = \|\widehat{\boldsymbol{\alpha}}\|_{2,1} \geq \|\widehat{\mathbf{X}}\|_* = \|\mathbf{X}\|_*$ by using the previous result derived in the square matrix case. A similar result is derived in the $m < n$ case.

Finally, the other mixed-norm $\|\boldsymbol{\theta}\|_{1,2}$ associated to $\mathbf{X}$ is equivalent to the mixed-norm $\|\boldsymbol{\theta}^\intercal\|_{2,1}$ associated to $\mathbf{X}^\intercal$. Now we using the same reasoning proved that $\|\boldsymbol{\theta}^\intercal\|_{2,1} \geq \|\mathbf{X}^\intercal\|_*$. So, since $\|\mathbf{X}^\intercal\|_* = \|\mathbf{X}\|_*$, we have $\|\boldsymbol{\theta}\|_{1,2} \geq \|\mathbf{X}\|_*$.

APPENDIX B

We are going to prove only the first result since the second one can be proved in the same way. So let's assume that $\mathbf{X}$ is full row rank.

On the one hand, we can easily derive from corollary 1 that $\frac{\|\mathbf{X}\|_{2,1}}{\|\mathbf{X}\|} \geq \frac{\|\mathbf{X}\|_*}{\|\mathbf{X}\|}$.

On the other hand, let's show that the rank of $\mathbf{X}$ is greater or equal than $\|\mathbf{X}\|_{2,1}/\|\mathbf{X}\|$. The SVD of $\mathbf{X}$ is given by $\mathbf{USV}^\intercal$ with $\mathbf{U} \in \mathbb{R}^{m \times m}$, $\mathbf{S} \in \mathbb{R}^{m \times n}$ and $\mathbf{V} \in \mathbb{R}^{n \times n}$. The mixed-norm $\|\mathbf{X}\|_{2,1}$ is equal to the summation of m terms $\|\mathbf{X}_{i,:}\|_2$, which can be computed as follows:

$$\|\mathbf{X}_{i,:}\|_2 = \sqrt{\mathbf{U}_{i,:}\mathbf{S}\mathbf{V}^\intercal\mathbf{V}\mathbf{S}^\intercal(\mathbf{U}_{i,:})^\intercal} = \sqrt{\mathbf{U}_{i,:}\mathbf{W}(\mathbf{U}_{i,:})^\intercal}$$

where $\mathbf{W} = \operatorname{diag}\big([s_1^2, \ldots, s_m^2]\big)$ is a diagonal matrix and where $(s_i)_{1 \leq i \leq m}$ denotes the set of singular values of $\mathbf{X}$ sorted in decreasing order. Then we have:

$$\begin{aligned}
\frac{\|\mathbf{X}_{i,:}\|_2}{\|\mathbf{X}\|} &= \frac{\sqrt{\mathbf{U}_{i,:}\mathbf{W}\mathbf{U}_{i,:}^\intercal}}{\|\mathbf{X}\|} = \sqrt{\frac{\mathbf{U}_{i,1}^2 s_1^2}{s_1^2} + \ldots + \frac{\mathbf{U}_{i,m}^2 s_m^2}{s_1^2}} \\
&\leq \sqrt{\mathbf{U}_{i,1}^2 + \ldots + \mathbf{U}_{i,m}^2} = 1
\end{aligned}$$

with $\|\mathbf{X}\| = s_1$. So we obtain:

$$\frac{\|\mathbf{X}\|_{2,1}}{\|\mathbf{X}\|} = \sum_{i=1}^{m} \frac{\|\mathbf{X}_{i,:}\|_2}{\|\mathbf{X}\|} \leq m = \operatorname{rank}(\mathbf{X})$$

REFERENCES

[1] T. G. Kolda and B. W. Bader, "Tensor decompositions and applications," *SIAM review*, vol. 51, no. 3, pp. 455–500, 2009.

[2] J. Liu, P. Musialski, P. Wonka, and J. Ye, "Tensor completion for estimating missing values in visual data," *IEEE Transactions on Pattern Analysis and Machine Intelligence*, vol. 35, no. 1, pp. 208–220, 2013.

[3] Y.-L. Chen, C.-T. Hsu, and H.-Y. M. Liao, "Simultaneous tensor decomposition and completion using factor priors," *IEEE Transactions on Pattern Analysis and Machine Intelligence*, vol. 36, no. 3, pp. 577–591, 2014.

[4] Y. Peng, D. Meng, Z. Xu, C. Gao, Y. Yang, and B. Zhang, "Decomposable nonlocal tensor dictionary learning for multispectral image denoising," in *IEEE Conference on Computer Vision and Pattern Recognition*, 2014, pp. 2949–2956.

[5] Q. Xie, Q. Zhao, D. Meng, Z. Xu, S. Gu, W. Zuo, and L. Zhang, "Multispectral images denoising by intrinsic tensor sparsity regularization," in *IEEE Conference on Computer Vision and Pattern Recognition*, 2016, pp. 1692–1700.

[6] T. Yokota, Q. Zhao, and A. Cichocki, "Smooth parafac decomposition for tensor completion," *IEEE Transactions on Signal Processing*, vol. 64, no. 20, pp. 5423–5436, 2015.

[7] C. Lu, J. Feng, Y. Chen, W. Liu, Z. Lin, and S. Yan, "Tensor robust principal component analysis: Exact recovery of corrupted low-rank tensors via convex optimization," in *IEEE Conference on Computer Vision and Pattern Recognition*, 2016, pp. 5249–5257.

[8] Y. Liu, F. Shang, W. Fan, J. Cheng, and H. Cheng, "Generalized higher order orthogonal iteration for tensor learning and decomposition," *IEEE transactions on neural networks and learning systems*, vol. 27, no. 12, pp. 2551–2563, 2016.

[9] D. Tao, X. Li, X. Wu, and S. J. Maybank, "General tensor discriminant analysis and gabor features for gait recognition," *IEEE Transactions on Pattern Analysis and Machine Intelligence*, vol. 29, no. 10, 2007.

[10] Z. Lai, W. K. Wong, Y. Xu, C. Zhao, and M. Sun, "Sparse alignment for robust tensor learning," *IEEE transactions on neural networks and learning systems*, vol. 25, no. 10, pp. 1779–1792, 2014.

[11] H. Becker, L. Albera, P. Comon, M. Haardt, G. Birot, F. Wendling, M. Gavaret, C.-G. Bénar, and I. Merlet, "EEG extended source localization: tensor-based vs. conventional methods," *NeuroImage*, vol. 96, pp. 143–157, 2014.

[12] H. Becker, L. Albera, P. Comon, R. Gribonval, F. Wendling, and I. Merlet, "Brain-source imaging: From sparse to tensor models," *IEEE Signal Processing Magazine*, vol. 32, no. 6, pp. 100–112, 2015.

[13] L. De Lathauwer, B. De Moor, and J. Vandewalle, "On the best rank-1 and rank-$(R_1, R_2, ..., R_n)$ approximation of higher-order tensors," *SIAM Journal on Matrix Analysis and Applications*, vol. 21, no. 4, pp. 1324–1342, 2000.

[14] L. De Lathauwer, "Decompositions of a higher-order tensor in block terms—part I: Lemmas for partitioned matrices," *SIAM Journal on Matrix Analysis and Applications*, vol. 30, no. 3, pp. 1022–1032, 2008.

[15] L. De Lathauwer, B. De Moor, and J. Vandewalle, "A multilinear singular value decomposition," *SIAM journal on Matrix Analysis and Applications*, vol. 21, no. 4, pp. 1253–1278, 2000.

[16] L. De Lathauwer, "Decompositions of a higher-order tensor in block terms—part II: Definitions and uniqueness," *SIAM Journal on Matrix Analysis and Applications*, vol. 30, no. 3, pp. 1033–1066, 2008.

[17] L. De Lathauwer and D. Nion, "Decompositions of a higher-order tensor in block terms—part III: Alternating least squares algorithms," *SIAM journal on Matrix Analysis and Applications*, vol. 30, no. 3, pp. 1067–1083, 2008.

[18] L. R. Tucker, "Implications of factor analysis of three-way matrices for measurement of change," *Problems in measuring change*, pp. 122–137, 1963.

[19] G. Schwarz *et al.*, "Estimating the dimension of a model," *The annals of statistics*, vol. 6, no. 2, pp. 461–464, 1978.

[20] T. P. Minka, "Automatic choice of dimensionality for PCA," in *Advances in neural information processing systems*, 2001, pp. 598–604.

[21] M. Wax and T. Kailath, "Detection of signals by information theoretic criteria," *IEEE Transactions on Acoustics, Speech, and Signal Processing*, vol. 33, no. 2, pp. 387–392, 1985.

[22] J. Rissanen, "Modeling by shortest data description," *Automatica*, vol. 14, no. 5, pp. 465–471, 1978.

[23] G. Zhou and A. Cichocki, "TDALAB: Tensor decomposition laboratory," *LABSP, Wako-shi, Japan*, 2013.

[24] J. Niesing, *Simultaneous component and factor analysis methods for two or more groups: a comparative study*. DSWO Press Leiden, The Netherlands, 1997.

[25] H. F. Kaiser, "The application of electronic computers to factor analysis," *Educational and psychological measurement*, vol. 20, no. 1, pp. 141–151, 1960.

[26] M. E. Timmerman and H. A. Kiers, "Three-mode principal components analysis: Choosing the numbers of components and sensitivity to local optima," *British journal of mathematical and statistical psychology*, vol. 53, no. 1, pp. 1–16, 2000.

[27] N. Vervliet, O. Debals, L. Sorber, M. Van Barel, and L. De Lathauwer, "Tensorlab 3.0," *available online, URL: www. tensorlab. net*, 2016.

[28] T. Yokota, N. Lee, and A. Cichocki, "Robust multilinear tensor rank estimation using higher order singular value decomposition and information criteria," *IEEE Transactions on Signal Processing*, vol. 65, no. 5, pp. 1196–1206, 2017.

[29] N. Renard, S. Bourennane, and J. Blanc-Talon, "Denoising and dimensionality reduction using multilinear tools for hyperspectral images," *IEEE Geoscience and Remote Sensing Letters*, vol. 5, no. 2, pp. 138–142, 2008.

[30] X. Liu, S. Bourennane, and C. Fossati, "Denoising of hyperspectral images using the PARAFAC model and statistical performance analysis," *IEEE Transactions on Geoscience and Remote Sensing*, vol. 50, no. 10, pp. 3717–3724, 2012.

[31] Z. Zhang, G. Ely, S. Aeron, N. Hao, and M. Kilmer, "Novel methods for multilinear data completion and de-noising based on tensor-SVD," in *Proceedings of the IEEE Conference on Computer Vision and Pattern Recognition*, 2014, pp. 3842–3849.

[32] M. Golbabaee and P. Vandergheynst, "Joint trace/TV norm minimization: A new efficient approach for spectral compressive imaging," in *Image Processing (ICIP), 2012 19th IEEE International Conference on*. IEEE, 2012, pp. 933–936.

[33] Q. Xie, Q. Zhao, D. Meng, and Z. Xu, "Kronecker-basis-representation based tensor sparsity and its applications to tensor recovery," *IEEE Transactions on Pattern Analysis and Machine Intelligence*, 2017.

[34] M. Aharon, M. Elad, and A. Bruckstein, "K-SVD: An algorithm for designing overcomplete dictionaries for sparse representation," *IEEE Transactions on signal processing*, vol. 54, no. 11, pp. 4311–4322, 2006.

[35] M. Elad and M. Aharon, "Image denoising via sparse and redundant representations over learned dictionaries," *IEEE Transactions on Image processing*, vol. 15, no. 12, pp. 3736–3745, 2006.

[36] K. Dabov, A. Foi, V. Katkovnik, and K. Egiazarian, "Image denoising by sparse 3-d transform-domain collaborative filtering," *IEEE Transactions on image processing*, vol. 16, no. 8, pp. 2080–2095, 2007.

[37] M. Maggioni and A. Foi, "Nonlocal transform-domain denoising of volumetric data with groupwise adaptive variance estimation." in *Computational Imaging*, 2012, p. 82960O.

[38] M. Maggioni, V. Katkovnik, K. Egiazarian, and A. Foi, "Nonlocal transform-domain filter for volumetric data denoising and reconstruction," *IEEE transactions on image processing*, vol. 22, no. 1, pp. 119–133, 2013.

[39] J. V. Manjón, P. Coupé, L. Martí-Bonmatí, D. L. Collins, and M. Robles, "Adaptive non-local means denoising of MR images with spatially varying noise levels," *Journal of Magnetic Resonance Imaging*, vol. 31, no. 1, pp. 192–203, 2010.

[40] B. Recht, M. Fazel, and P. A. Parrilo, "Guaranteed minimum-rank solutions of linear matrix equations via nuclear norm minimization," *SIAM review*, vol. 52, no. 3, pp. 471–501, 2010.

[41] M. Fazel, "Matrix rank minimization with applications," Ph.D. dissertation, PhD thesis, Stanford University, 2002.

[42] B. Huang, C. Mu, D. Goldfarb, and J. Wright, "Provable low-rank tensor recovery," *Optimization-Online*, vol. 4252, p. 116, 2014.

[43] P. Shah, N. Rao, and G. Tang, "Sparse and low-rank tensor decomposition," in *Advances in Neural Information Processing Systems*, 2015, pp. 2548–2556.

[44] J.-F. Cai, E. J. Candès, and Z. Shen, "A singular value thresholding algorithm for matrix completion," *SIAM Journal on Optimization*, vol. 20, no. 4, pp. 1956–1982, 2010.

[45] D. Zhang, Y. Hu, J. Ye, X. Li, and X. He, "Matrix completion by truncated nuclear norm regularization," in *IEEE Conference on Computer Vision and Pattern Recognition*. IEEE, 2012, pp. 2192–2199.

[46] Y. Hu, D. Zhang, J. Ye, X. Li, and X. He, "Fast and accurate matrix completion via truncated nuclear norm regularization," *IEEE Transactions on Pattern Analysis and Machine Intelligence*, vol. 35, no. 9, pp. 2117–2130, 2013.

[47] T.-H. Oh, H. Kim, Y.-W. Tai, J.-C. Bazin, and I. So Kweon, "Partial sum minimization of singular values in rpca for low-level vision," in *IEEE international conference on computer vision*, 2013, pp. 145–152.

[48] T.-H. Oh, Y.-W. Tai, J.-C. Bazin, H. Kim, and I. S. Kweon, "Partial sum minimization of singular values in robust pca: Algorithm and applications," *IEEE transactions on pattern analysis and machine intelligence*, vol. 38, no. 4, pp. 744–758, 2016.

[49] X. Shu, F. Porikli, and N. Ahuja, "Robust orthonormal subspace learning: Efficient recovery of corrupted low-rank matrices," in *Proceedings of the IEEE Conference on Computer Vision and Pattern Recognition*, 2014, pp. 3874–3881.

[50] E. J. Candes, M. B. Wakin, and S. P. Boyd, "Enhancing sparsity by reweighted l_1 minimization," *Journal of Fourier analysis and applications*, vol. 14, no. 5, pp. 877–905, 2008.

[51] D. L. Donoho and I. M. Johnstone, "Adapting to unknown smoothness via wavelet shrinkage," *Journal of the american statistical association*, vol. 90, no. 432, pp. 1200–1224, 1995.

[52] E. T. Hale, W. Yin, and Y. Zhang, "Fixed-point continuation for l_1-minimization: Methodology and convergence," *SIAM Journal on Optimization*, vol. 19, no. 3, pp. 1107–1130, 2008.

[53] S. Boyd, N. Parikh, E. Chu, B. Peleato, and J. Eckstein, "Distributed optimization and statistical learning via the alternating direction method of multipliers," *Foundations and Trends® in Machine Learning*, vol. 3, no. 1, pp. 1–122, 2011.

[54] Z. Lin, M. Chen, and Y. Ma, "The augmented lagrange multiplier method for exact recovery of corrupted low-rank matrices," *Technical report, UILU-ENG-09-2215*, 2009.
[55] K. B. Petersen, M. S. Pedersen *et al.*, "The matrix cookbook," *Technical University of Denmark*, vol. 7, p. 15, 2008.
[56] L. Mirsky, "A trace inequality of john von neumann," *Monatshefte für mathematik*, vol. 79, no. 4, pp. 303–306, 1975.
[57] B. He and X. Yuan, "On the o(1/n) convergence rate of the douglas–rachford alternating direction method," *SIAM Journal on Numerical Analysis*, vol. 50, no. 2, pp. 700–709, 2012.
[58] R. Bro, "Parafac. tutorial and applications," *Chemometrics and intelligent laboratory systems*, vol. 38, no. 2, pp. 149–171, 1997.
[59] F. Yasuma, T. Mitsunaga, D. Iso, and S. K. Nayar, "Generalized assorted pixel camera: postcapture control of resolution, dynamic range, and spectrum," *IEEE transactions on image processing*, vol. 19, no. 9, pp. 2241–2253, 2010.
[60] Z. Wang, A. C. Bovik, H. R. Sheikh, and E. P. Simoncelli, "Image quality assessment: from error visibility to structural similarity," *IEEE transactions on image processing*, vol. 13, no. 4, pp. 600–612, 2004.

Amar Kachenoura (Tasks 1, 2 and 3) was born in Tizi-Ouzou, Algeria, in 1975. He received the diploma in electronic engineering from M.M.T.O. University, Tizi-Ouzou, Algeria, in 1998 and the DEA degree from Ecole Central de Nantes (ECN), Nantes, France, in July 2002. He received the Ph.D. degree in signal processing from the University of Rennes 1, Rennes, France, in July 2006. He is currently Engineer researcher at University of Rennes 1 and is affiliated with the INSERM research group LTSI (Laboratoire Traitement du Signal et de l'Image). His research interests focus mainly on statistical signal processing, blind source separation, independent component analysis, non linear and non stationary signals analysis, high order statistics and analysis, and interpretation of biosignals (Electrocardiography, Electroencephalography, and NMR Spectroscopy). He has co-authored 5 patents and about 60 research papers in journals, conferences and books chapter. He is also a regular reviewer for international journals (Signal image and video processing, Elsevier Signal Processing, etc).

Xu Han received the M.S. degree in engineering from the School of Biological Sciences and Medical Engineering, Southeast University, Nanjing, China, in 2014. He is currently working toward the PhD degree in signal processing and telecommunication at the Laboratoire du Traitement du Signal et de l'Image (LTSI). His research interests include tensor decomposition, convex optimization and image processing.

Huazhong Shu (M'00–SM'06) received the B.S. degree in Applied Mathematics from Wuhan University, China, in 1987, and a Ph.D. degree in Numerical Analysis from the University of Rennes 1, Rennes, France in 1992. He is a professor of the LIST Laboratory, Southeast University, Nanjing, China and the Co-director of the CRIBs. His recent work concentrates on the image analysis, pattern recognition and fast algorithms of digital signal processing. Prof. Shu is a senior member of IEEE Society.

Laurent Albera was born in Massy, France, in 1976. After a DESS in Mathematics, He received in 2001 the DEA's degree in Automatic and Signal Processing from the University of Science of Orsay (Paris XI). From 2001 to 2004, he was committed for a study within the framework of a Research Contract CIFRE (Convention Industrielle de Formation par la Recherche) between Thales Communications (formerly Thomson-CSF), the french National Centre for Scientific Research CNRS and the University of Nice Sophia-Antipolis. He received in 2003 the PH.D. degree in Sciences form the University of Nice Sophia-Antipolis, France. He received in 2010 the H.D.R. (Habilitation to Lead Researches) degree in Sciences from the University of Rennes 1, France. He is Assistant Professor at the University of Rennes 1 and is affiliated with the INSERM research group LTSI (Laboratoire Traitement du Signal et de l'Image) since 2004. His research interests include high-order statistics, multidimensional algebra, blind source separation, statistical signal and array processing, and numerical analysis. More particularly, Laurent Albera is currently working on numerical methods for tensor decompositions and applications in biomedical engineering.

Lotfi Senhadji (M'95–SM'99) received the Ph.D. degree from the University of Rennes 1, Rennes, France, in signal processing and telecommunications in 1993. He is a Professor and the Head of the INSERM Research Laboratory LTSI. He is also Co-Director of the French-Chinese Laboratory CRIBs "Centre de Recherche en Information Biomédicale Sino-Français". His main research efforts are focused on signal processing and modeling for detection, estimation, classification, interpretation of biosignals. He has published more than 100 research papers in journals and conferences, and he contributed to several handbooks. Prof.Senhadji is a senior member of the IEEE EMBS and the IEEE Signal Processing Society.

TABLE 1: The PSNR and SSIM results of 4 methods with respect to the selected 30 Columbian MSI images under different variances and the best PQI result of each MSI image is highlighted in bold.

	PSNR					SSIM				
v=0.1	noisy	SCORE+T-HOSVD	SCORE+HOOI	KBR	R-OMTD	noisy	SCORE+T-HOSVD	SCORE+HOOI	KBR	R-OMTD
chart and stuffed toy	19.9958	39.7933	40.2741	39.7312	**41.3866**	0.1821	0.9565	0.9708	0.9500	**0.9757**
face	19.9958	41.4302	43.0097	41.1423	**43.4531**	0.0996	0.9488	0.9727	0.9300	**0.9761**
lemon slices	19.9958	40.1221	41.2037	40.5672	**41.4984**	0.1236	0.9446	0.9625	0.9529	**0.9651**
feathers	19.9958	39.5651	39.7819	39.9841	**40.7154**	0.1615	0.9572	0.9640	0.9603	**0.9683**
peppers	19.9958	41.8061	43.0135	42.2541	**43.9491**	0.1013	0.9530	0.9714	0.9594	**0.9759**
balloons	19.9958	42.5785	42.6891	42.7507	**43.9987**	0.1112	0.9797	0.9820	0.9763	**0.9869**
beads	19.9958	36.8233	36.9349	36.5799	**37.2466**	0.2879	0.9537	0.9546	0.9560	**0.9622**
cd	19.9958	40.5194	40.5495	40.5491	**41.3909**	0.0979	0.9503	0.9525	0.9451	**0.9581**
clay	19.9958	43.7046	44.6540	42.3656	**45.7426**	0.0797	0.9567	0.9706	0.9121	**0.9764**
cloth	19.9958	35.0465	**35.4958**	34.3354	35.1905	0.3362	0.9270	**0.9368**	0.9242	0.9301
egyptian	19.9958	42.8430	42.9004	42.0138	**43.9231**	0.0830	0.9359	0.9502	0.8861	**0.9618**
beers	19.9958	41.4590	41.3415	41.5460	**42.2369**	0.1279	0.9796	0.9773	0.9735	**0.9819**
lemons	19.9958	42.6618	43.9997	42.8139	**44.4421**	0.0944	0.9634	0.9766	0.9637	**0.9786**
strawberries	19.9958	40.9475	42.4197	41.4558	**42.4515**	0.1020	0.9454	0.9653	0.9538	**0.9655**
sushi	19.9958	42.1991	43.8728	42.6492	**44.9820**	0.0830	0.9563	0.9800	0.9619	**0.9832**
tomatoes	19.9958	41.9295	43.4204	41.2409	**43.9886**	0.0825	0.9464	0.9740	0.9296	**0.9772**
flowers	19.9958	40.4793	40.7844	40.1102	**41.6101**	0.1218	0.9498	0.9566	0.9119	**0.9632**
glass tiles	19.9958	39.4512	39.5204	39.5659	**40.4281**	0.1987	0.9579	0.9633	0.9591	**0.9682**
hairs	19.9958	39.7013	**40.6926**	40.0929	40.6626	0.1226	0.9338	**0.9501**	0.9411	0.9486
jelly beans	19.9958	38.1193	38.2048	38.0110	**38.7876**	0.2564	0.9614	0.9632	0.9621	**0.9678**
oil painting	19.9958	36.1677	**36.8361**	36.2648	36.5549	0.2066	0.9158	**0.9300**	0.9192	0.9233
paints	19.9958	40.6388	40.6843	40.7993	**41.9878**	0.2220	0.9777	0.9808	0.9743	**0.9845**
photo and face	19.9958	42.1708	42.9240	40.9757	**43.4144**	0.1135	0.9581	0.9716	0.8507	**0.9754**
pompoms	19.9958	38.0097	38.0286	**38.3991**	38.3301	0.1678	0.9365	0.9354	**0.9390**	0.9384
sponges	19.9958	43.5206	43.6902	42.9192	**44.2709**	0.1303	0.9828	0.9834	0.9736	**0.9851**
stuffed toy	19.9958	40.4260	40.2166	40.5905	**42.0775**	0.1401	0.9521	0.9623	0.9433	**0.9710**
superballs	19.9958	41.5433	42.7069	42.0630	**43.5970**	0.0842	0.9397	0.9579	0.9468	**0.9622**
thread spools	19.9958	40.1077	40.5277	40.5523	**41.5995**	0.1395	0.9427	0.9589	0.9491	**0.9638**
watercolors	19.9958	36.9339	37.0661	36.9350	**37.6065**	0.2567	0.9514	0.9525	0.9514	**0.9572**
yellow peppers	19.9958	42.6862	43.5648	42.7779	**44.3277**	0.1038	0.9702	0.9781	0.9678	**0.9815**
v=0.2										
chart and stuffed toy	13.9752	35.4606	36.2556	35.6540	**36.8434**	0.0763	0.9208	0.9373	0.8739	**0.9449**
face	13.9752	37.4225	38.3599	37.3051	**38.9100**	0.0279	0.9136	0.9354	0.8196	**0.9435**
lemon slices	13.9752	36.0875	37.6200	36.9001	**37.9200**	0.0384	0.8981	0.9306	0.9085	**0.9365**
feathers	13.9752	35.3364	36.3425	36.1740	**36.9211**	0.0623	0.9106	0.9356	0.9226	**0.9415**
peppers	13.9752	37.0021	38.6036	37.9789	**39.2447**	0.0297	0.8992	0.9339	0.9107	**0.9412**
balloons	13.9752	37.0157	38.1641	38.1596	**39.1034**	0.0321	0.9409	0.9580	0.9503	**0.9666**
beads	13.9752	32.6301	33.3342	32.7973	**33.5303**	0.1273	0.9039	0.9182	0.9130	**0.9265**
cd	13.9752	35.8795	37.3211	37.3558	**38.0847**	0.0260	0.8894	0.9251	0.9158	**0.9339**
clay	13.9752	39.6723	39.5723	39.0381	**40.7244**	0.0218	0.8927	0.9172	0.7987	**0.9388**
cloth	13.9752	30.6578	**31.3704**	30.6897	31.3201	0.1347	0.8406	**0.8596**	0.8484	0.8575
egyptian	13.9752	38.6433	38.1015	**38.7464**	38.3292	0.0228	0.8719	0.8788	0.8426	**0.8913**
beers	13.9752	37.4609	37.6150	37.7307	**38.2320**	0.0405	0.9659	0.9639	0.9583	**0.9705**
lemons	13.9752	37.2558	39.5769	38.7635	**40.0162**	0.0255	0.9095	0.9494	0.9282	**0.9538**
strawberries	13.9752	36.6063	38.4169	37.5181	**38.6437**	0.0288	0.8895	0.9252	0.9007	**0.9297**
sushi	13.9752	37.3531	40.2775	39.0046	**40.8974**	0.0210	0.8952	0.9570	0.9239	**0.9603**
tomatoes	13.9752	37.7481	39.4715	38.0636	**39.8217**	0.0232	0.8973	0.9377	0.8778	**0.9392**
flowers	13.9752	36.3347	36.9132	36.5891	**37.4872**	0.0379	0.8914	0.9037	0.8468	**0.9140**
glass tiles	13.9752	35.2123	36.2476	35.9826	**36.8623**	0.0851	0.9214	0.9419	0.9324	**0.9495**
hairs	13.9752	35.5380	37.3875	36.7878	**37.5397**	0.0376	0.8700	0.9149	0.8960	**0.9170**
jelly beans	13.9752	33.4745	34.3114	33.9158	**34.7987**	0.1093	0.9084	0.9245	0.9212	**0.9346**
oil painting	13.9752	32.4345	33.3541	33.1778	**33.4276**	0.0708	0.8329	0.8610	0.8551	**0.8620**
paints	13.9752	35.2651	36.5166	36.5298	**37.4659**	0.0980	0.9345	0.9587	0.9503	**0.9660**
photo and face	13.9752	37.6335	37.8324	37.6934	**38.4673**	0.0337	0.8847	0.9018	0.7775	**0.9263**
pompoms	13.9752	34.7422	35.2318	35.3706	**35.7423**	0.0523	0.9019	0.9068	0.9084	**0.9161**
sponges	13.9752	38.9169	39.9722	39.3855	**40.4566**	0.0453	0.9652	0.9721	0.9599	**0.9758**
stuffed toy	13.9752	36.7063	37.1675	37.0762	**38.1285**	0.0469	0.9176	0.9312	0.8964	**0.9415**
superballs	13.9752	37.0611	39.1894	38.4002	**39.8679**	0.0214	0.8844	0.9292	0.9046	**0.9351**
thread spools	13.9752	36.0790	37.0615	36.8120	**37.8739**	0.0472	0.8965	0.9215	0.9002	**0.9311**
watercolors	13.9752	32.7293	33.7177	33.3585	**33.9061**	0.1085	0.9091	0.9224	0.9183	**0.9281**
yellowpeppers	13.9752	37.2142	39.3202	38.6478	**39.7607**	0.0298	0.9176	0.9529	0.9353	**0.9578**